AD-A134 182 DETERMINATION OF INDIVIDUAL TEMPERATURES AND LUMINOSITIES IN ECLIPSING BINARY STAR SYSTEMS(U) NAVAL ACADEMY ANNAPOLIS MD R M CAMPBELL 20 JUN 83 1/2

UNCLASSIFIED USNA-TSPR-122 F/G 3/2 NL

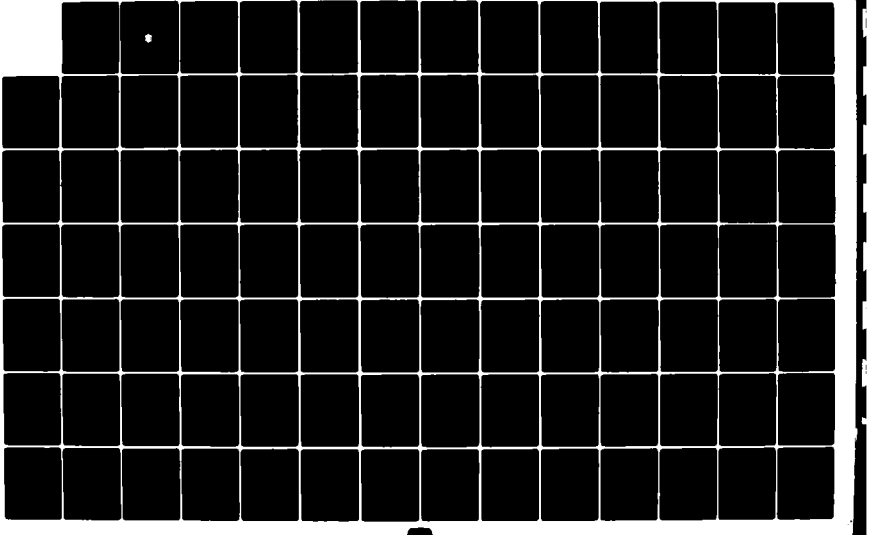

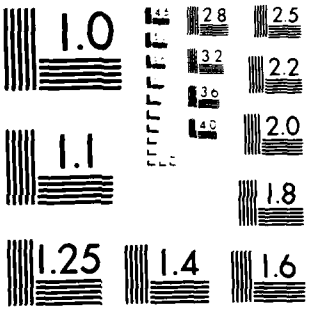

A134 182

(20)

# A TRIDENT SCHOLAR PROJECT REPORT

NO. 122

## DETERMINATION OF INDIVIDUAL TEMPERATURES AND LUMINOSITIES IN ECLIPSING BINARY STAR SYSTEMS

UNITED STATES NAVAL ACADEMY
ANNAPOLIS, MARYLAND
1983

# DETERMINATION OF INDIVIDUAL TEMPERATURES AND LUMINOSITIES IN ECLIPSING BINARY STAR SYSTEMS

A Trident Scholar Project Report

by

Midshipman Robert M. Campbell, Class of 1983

U.S. Naval Academy

Annapolis, Maryland

Graham D. Gutsche

Professor Graham D. Gutsche

Physics Department

Accepted for Trident Scholar Committee

Charles F Rawell

Chairman

June 20, 1983

Date

TABLE OF CONTENTS

ABSTRACT.....1

ACKNOWLEDGEMENTS.....2

I. THEORETICAL CONSIDERATIONS.....3

Single Stars. . . . . .3
Binary Stars. . . . . 16

II. EXPERIMANTAL DESIGN.....27

III. GENERATION OF RESULTS.....42

IV. DATA AND INTERPRETATION.....52

V. CONCLUSIONS.....82

FOOTNOTES.....84

BIBLIOGRAPHY.....86

APPENDIX I: Nuclear Fuel Cycles.....88

APPENDIX II: Computer Programs.....91

APPENDIX III: Star Lists.....99

APPENDIX IV: Standard Star Observations.....101

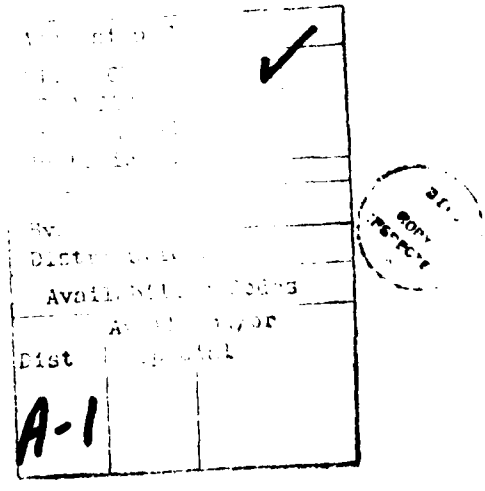

## ABSTRACT

The purpose of this project was to determine the temperatures and luminosities of the individual components of eclipsing binary star systems. Dr. Richard L. Walker of the U.S. Naval Observatory provided a list of such systems which were as yet undetermined. The information sought was gained by UBV photometry of a system at total eclipse and at a time outside eclipse. The light at totality is due entirely to the occulting star, and outside eclipse, both stars contribute fully. A method is derived for subtracting out the light of the occulting star to obtain measurements of the occulted.

A recently published technique by William E. Harris was used to reduce raw observational data. Essentially a simultaneous, multi-linear solution for both atmospheric extinction and instrumental transformation, this method was programmed onto the Naval Academy's extensive computing facilities. It was found that this method, as claimed, gives accurate results with a minimum of time and effort, upon completion of the initial phase of programming.

Systems for which a complete solution (temperature and luminosity of both components) was reached include: TU Camelopardi, TW Draconis, AK Herculis, V566 Ophiuchi, W Ursae Majoris, and AG Virginis. Systems observed only during totality, thus solving only the occulting star, include α Corona Borealis and AM Leonis. RS Canes Venatici and TZ Bootes were observed only out of eclipse, and must await further study. Once a solution for a system was obtained, it was presented graphically on a Hertzsprung-Russell diagram, and was examined from the viewpoint of binary evolution.

## ACKNOWLEDGEMENTS

The author is deeply obliged to Dr. Graham D. Gutsche of the U.S. Naval Academy Physics Department, without whose insight and advice this project would have been rendered astronomically more difficult. Gratitude is also extended to Messrs. Norm Stead and Clarence Meekins of the Physics Department technical staff for the Herculean achievement of bringing and maintaining the telescope and supporting systems to operational levels. Special thanks also go to Dr. Richard L. Walker of the U.S. Naval Observatory, Flagstaff Station, for guidance in the initial phases of the project, to Drs. C. Elise Albert and Irene M. Engle for supplying answers to miscellaneous questions throughout the year, and to Patricia M. Kelly and Brenda Davis for unlocking the wonders of word processing.

# I - THEORETICAL CONSIDERATIONS

A primary goal of binary star astronomy is to understand the circumstances and mechanisms which led to their formation and which will dictate their future. Definitive solutions to these problems clearly do not yet exist, and are for the most part beyond the scope of this paper. Yet, to make any real progress in this direction, one requires a firm grasp of the nature of binary stars. This section will therefore discuss the dynamics, physical characteristics, and evolution of binary systems, prefaced by a treatment of similar topics for ordinary single stars, since these form the components of binary systems. These theoretical considerations will then lay the foundation for interpretation of experimental results and hopefully lead to insights into binary system development.

## Single Stars

For the purposes of this paper, stars possess two essential properties. The first of these is temperature. Unfortunately, the most crucial temperature, that which controls the type and rate of energy generation, remains unobservable in the central regions of the star. On Earth, one can measure only the temperature at the depth in from the surface at which the star becomes opaque to the wavelength of light observed. If we limit the range of wavelengths to the visible and the near ultra-violet regions, the differences in penetration depths relative to stellar radii becomes insignificant, and we have defined a useful measure of temperature with which to compare stars, the effective temperature.

There are several alternative measures of temperature. Spectral class orders stars by the characteristics of their spectra, which depend in turn on the excitation levels of the various atoms in their atmosphere. This is a standard way to specify temperature, primarily for economy of print. The spectral classes are described in table 1-1.

TABLE 1-1

| SPECTRAL CLASS | $T(\times 10^3 K)$ | CHARACTERISTICS |
|---|---|---|
| O5 | 50.0 | Absorption: ionized $He^3$, N, O, Si |
| B0 | 27.0 | Absorption: $He^4$ |
| B5 | 16.0 | $He^4$ declining, Balmer series increasing |
| A0 | 10.4 | No He lines, H lines dominant |
| A5 | 8.2 | Singly ionized Ca increasing |
| F0 | 7.2 | H weakening, Ca increasing |
| F5 | 6.7 | Neutral metal lines increasing |
| G0 | 6.0 | Ca strong, many neutral metals |
| G5 | 5.5 | CN, CH molecular bands |
| K0 | 5.1 | Ca maximum, neutral metals stronger |
| K5 | 4.3 | Many molecules |
| M0 | 3.7 | Neutral metals intense, H weak |
| M5 | 3.0 | TiO appears |

Color also measures stellar temperatures, ranging from bluish-white for hot O and B stars to yellow for G stars (like the Sun) to red for cool M stars. Unfortunately, since determining the color of an unknown star is largely subjective, it is not a strictly precise temperature measurement. However, color index, the difference in intensities of starlight at two specified wavelengths, does give an accurate result to the approximation that stars radiate as black bodies. One color index uniquely determines a Planck curve, which specifies the temperature. Addition of a third wavelength (a second color index) shows that a star is

not a perfect black body, and reveals subtleties of the stellar atmosphere, which will later become quite important.

The second essential property of a star is its luminosity, the total energy emitted per unit time:

$$L=(4\pi r^2)(\sigma T^4) \qquad (1\text{-}1)$$

where $\sigma$ is the Stefan-Boltzmann constant. Since stellar radii are generally not known, this equation is of limited usefulness in finding luminosities.

The concept of stellar magnitudes allows one to obtain a usable measure of stellar luminosities. The magnitude scale ranks stars on the basis of visual response to their relative brightnesses. Due to ocular physiology, this scale is logarithmic:

$$m_2-m_1=2.5\log(L_1/L_2) \qquad (1\text{-}2)$$

We notice from this equation the unfortunate historic convention that brighter stars have lower magnitudes. A first magnitude star is one hundred times brighter than a sixth magnitude star.

Since the flux of stellar radiation obeys an inverse square law, stars closer to the Earth will appear unnaturally brighter than those further away. To equalize this distance dependency, we define absolute magnitude as the magnitude of a star if it were ten parsecs (about thirty-two light years) distant. As an example, the proximity of the Sun gives it an apparent magnitude of -26.8, whereas its absolute magnitude is only +4.8.

Once we know a star's temperature and luminosity, we can locate a star's position on a Hertzsprung-Russell diagram, a plot

of luminosity versus temperature, as in figure 1-1[1]. An important feature of this plot is that stars are not randomly distributed as one might expect, but rather group themselves along specific bands. These bands are termed luminosity classes, and are the subtle distinctions measured by a second color index.

The H-R diagram also gives a graphical representaiton of a star's evolution. At any time in its life, a star will occupy a specific position on the diagram. If we connect all the points of its lifetime, we obtain an evolutionary track. The next task is thus to approach these tracks theoretically, searching for the signifigance of and explanations for the grouping found on the H-R diagram.

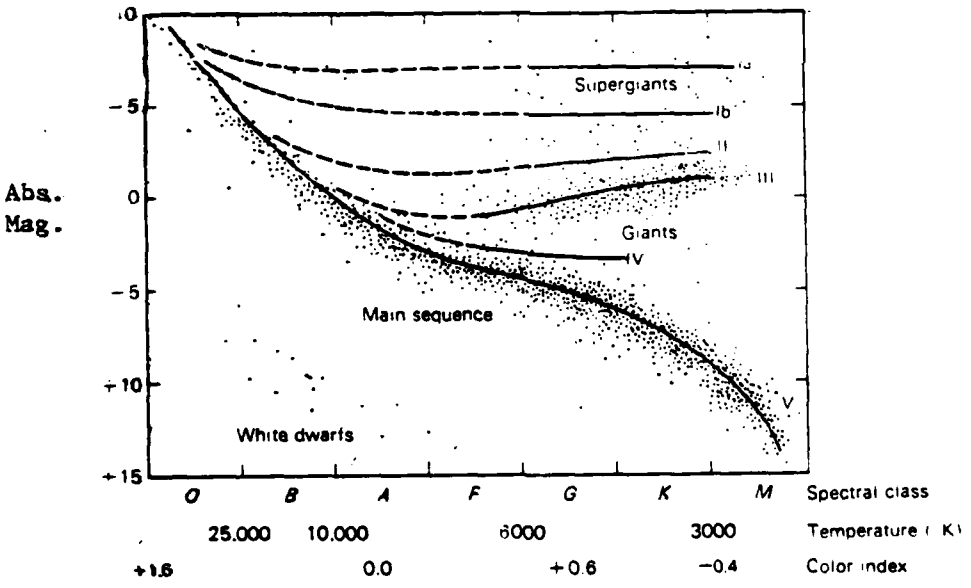


Figure 1-1.

It is generally accepted that stars originate in areas where the local density of interstellar gas and dust is high enough to initiate gravitational condensation. As this cloud contracts, its particles lose gravitational potential energy. The virial theorem for inverse square interactions:

$$\langle T \rangle = -\frac{1}{2}\langle U \rangle \qquad (1\text{-}3)$$

shows that half of this energy loss goes into increasing the average kinetic energy (i.e. the temperature) of the cloud. The other half must be radiated away. Initially, the mean free path of these photons is large, and they can escape from the cloud regardless of their depth of emission. This contraction stage is relatively rapid, on the order of $10^3$ years[2], less for more massive clouds and greater for lighter clouds.

At this time, however, the density of the proto-star has increased, lowering the mean free path of the photons such that they will most probably interact and release their energy well inside the proto-star. This radiation pressure increases the internal temperature and establishes a large inwardly increasing density gradient. The contraction also slows due to the radiation pressure until the internal temperature reaches 1300K, at which point $H_2$ dissociates[3] (endothermically), again allowing a rapid contraction. This phase continues until a state of approximate hydrostatic equilibrium is reached.

After about $10^7$ years, nuclear reactions begin to contribute to the proto-star's luminosity.[4] These reactions are only precursors to the eventual energy production mechanisms, since internal

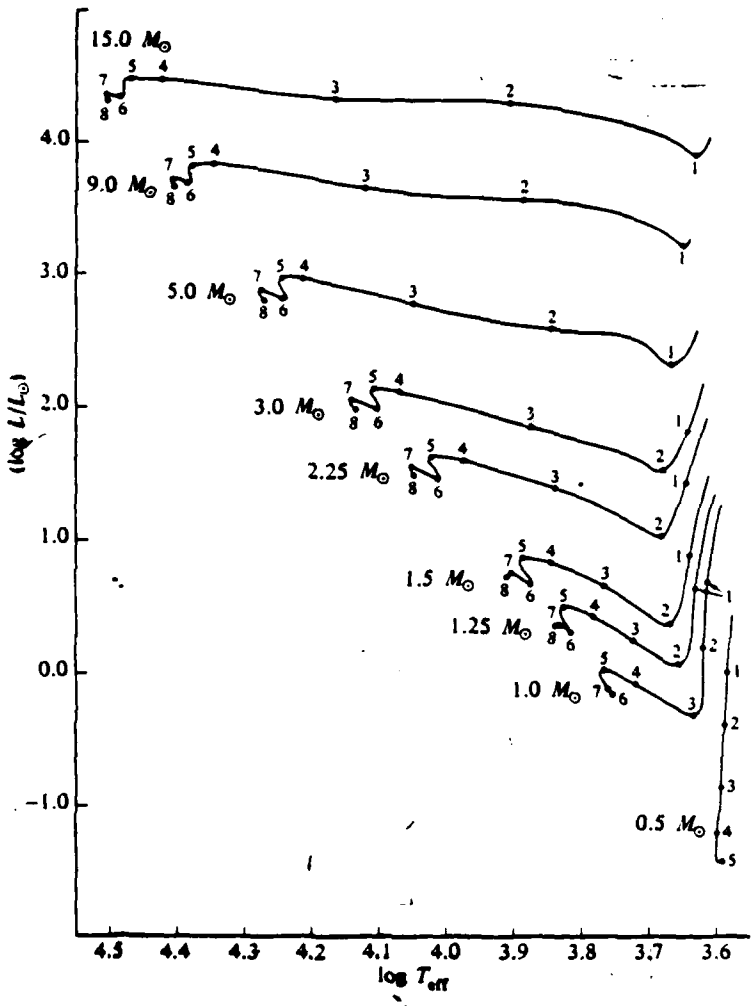


Figure 1-2. Pre-main sequence evolution on a H-R diagram.

temperatures are still too low to ignite complete fusion chains. Figure 1-2[5] gives a composite view of stellar life for masses from one-half to fifteen solar massses to this point.

Before following stellar evolution further, it is best to momentarily digress to the subject of degenerate matter and its effects on the subsequent life of stars. For an n-dimensional object, there exists a 2n-dimensional phase space whose co-ordinates are the n spatial co-ordinates ($q_i$) and the respective momenta co-ordinates ($p_i$). The Heisenberg uncertainty relationship between position and momentum gives the mimimun volume of a state in 2n space:

$$(\Pi\Delta q_i)(\Pi\Delta p_i) \geq (h/2\pi)^n \qquad (1\text{-}4)$$

into which no two fermions (spin one-half particles, for our purposes, electrons and neutrons) can be placed, due to Pauli exclusion. The available physical (spatial) volume is controlled by the particle density; an increase in density causes the average particle separation to decrease (decreasing $\Pi\Delta q_i$), limiting the number of available states. Likewise, volume in momentum space is controlled by temperature; an increase in temperature raises the average particular momentum, thereby increasing $\Pi\Delta p_i$. When all the available states for a given density and temperature are occupied, we have degenerate matter, and the particles exert a great pressure (degeneracy pressure) to avoid violating the Pauli exclusion principle.

Thus, a star isothermally contracting will eventually stop; the number of momentum states are constant, while the number of

spatial states decreases. The total number of states therefore decreases, while the number of particles remains the same, making electron degeneracy inevitable. However, if we increase the temperature, more momentum states become available, allowing the number of spatial states to continue to decrease. Thus we get the curious result that adding energy to degenerate matter causes a contraction, as long as degeneracy is not removed.

The proto-star we left in figure 1-2 now has two mass-dependent alternatives. If its mass is less than a tenth of a solar mass, the internal temperature never reaches the ignition point of hydrogen fusion. This "black dwarf" releases energy through the motion of its particles, gradually cooling to equilibrium with the space around it. If its mass is greater than this limit, the star will commence its long life of hydrogen burning.

The onset of hydrogen fusion is termed Zero Age Main Sequence. (The main sequence is the densely populated diagonal band on the H-R diagram. Most of the stars we see are on the main sequence simply because stars spend most of their lives burning hydrogen.) At this point, the chemical composition of the star can be considered homogeneous, with typical values of 71% H, 27% He, and 2% heavier elements, by weight.[6] The star generates energy by fusing four $H^1$ into one $He^4$, primarily by either the proton-proton chain or the carbon-nitrogen cycle (see Appendix I). The important feature of both reactions is that only 0.71% of the mass of the four hydrogens is converted into energy. Thus, during the main sequence, the stellar mass remains essentially constant, but the composition changes drastically.

As $4H^1 \rightarrow He^4$, the temperature decreases slightly due to the increased average molecular weight ($\mu$) of the gas as a whole, and the luminosity increases for the same reason. (L ranges in proportionality from $\mu^{7.5}$ in small stars to $\mu^4$ in large stars.[7]) The star thus moves upward and to the right a small amount while on the main sequence. The stellar mass determines the length of the star's stay here; more massive stars have higher internal temperatures, which causes a faster nuclear reaction rate and a more rapid hydrogen depletion. For the sun, this time would be about $9 \times 10^9$ years, and for a star five times as massive, $3 \times 10^7$ years.[8]

As time passes, hydrogen becomes exhausted in the central regions, leaving an inert helium core and a hydrogen burning shell around it. As more hydrogen is depleted, the helium core grows and eventually begins to gravitationally contract. This releases gravitational potential energy, which raises the temperature and the fusion rate of the burning shell. The increase in energy flux from this shell pushes the outer regions of the star away and forces the core in on itself. The surface temperature decreases with expansion, but the luminosity remains more or less constant due to the increase in the radiating area.

Meanwhile, the temperature and density of the contracting helium core continue to increase. It now has three mass and temperature dependent alternatives. If the star has less than half a solar mass, the core will be too cool to ignite helium burning, and will suffer electron degeneracy.[9] The outer layers will continue to expand, leaving behind a small, degenerate white dwarf. This releases energy through the motion of the non-degenerate

nuclei ($m_n \approx 2000 m_e$), and also cools to equilibrium with its surroundings.

If the star has more than three solar masses, central temperatures will be high enough to commence helium burning via the triple-alpha chain (see Appendix I). This new source of energy expands the core, which decreases its outward pressure, allowing the outer layers to re-contract. A rule of thumb for determining qualitatively the radius variation is that each nuclear burning shell reverses the direction of expansion or contraction, as illustrated in Figure 1-3.[10] The temperature in the core peaks and then decreases with expansion, and the luminosity decreases due to the blanketing effect of the cooler outer envelope. Yet, as the envelope contracts, it also heats, causing the luminosity to swing back up. Just as in the hydrogen burning phase, the helium eventually becomes depleted, leaving a predominantly carbon-oxygen inert core surrounded by a helium burning shell. This moves the peak temperature radially outward, further increasing the luminosity.

Stars between these two mass limits ($\frac{1}{2} m_o < m_* < 3 m_o$) reach the state previously described for massive stars, but through an entirely different mechanism. At the termination of hydrogen burning in these stars, the temperature is sufficiently low to allow the very central regions to become degenerate. The hydrogen burning shell pushes the core in on itself, starting minor helium burning. This added energy contracts the degenerate region, increasing its temperature and thus increasing the helium fusion rate. This cycle clearly establishes a volatile instability as long as some of the core remains degenerate. This is termed helium flash;

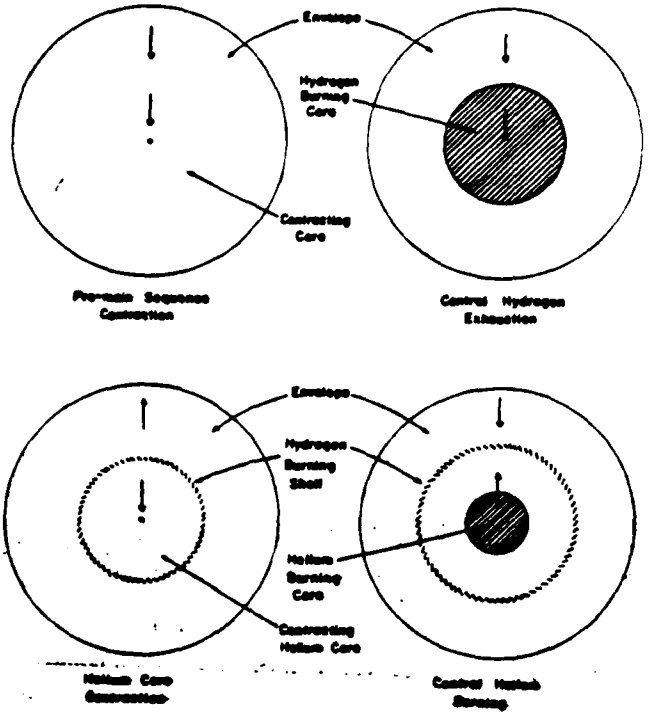


Figure 1-3. Effects of central activity on stellar radius.

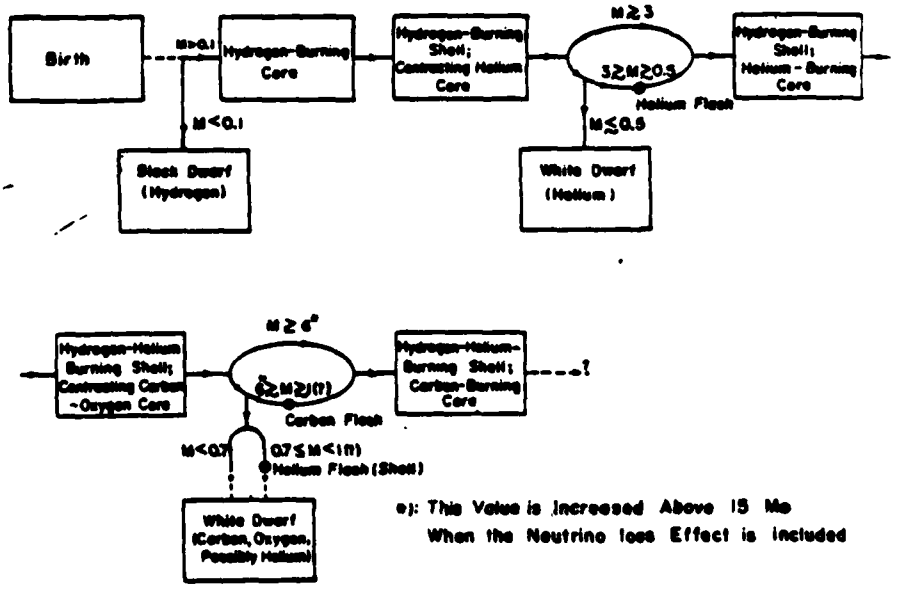


Figure 1-4. Evolutionary flowchart.

the power per unit mass released by such a core can reach $10^{14}$ erg/gm/s. The sun in contrast puts out 10 erg/gm/s.[11] The temperature soon increases enough to remove degeneracy, and the core expands and cools. The helium core now burns as does a more massive star's, leaving a carbon-oxygen inert core and a helium burning shell.

The star is now faced with three further mass dependent alternatives: a degenerate carbon-oxygen white dwarf, ignition of carbon burning, or carbon flash. In these stages, the energy loss through neutrinos has an appreciable affect on the critical masses; at least six solar masses are required to avoid carbon flash ignoring neutrino loss, but fifteen are required when it is included.[12] Figure 1-4 summarizes the evolutionary stages related to this study. Figure 1-5[13] shows the evolutionary tracks of stars of various masses from Zero Age Main Sequence.

We can see from Figure 1-5 that stars of moderate masses all move into the giant region, and very massive stars become supergiants. For stars less than three solar masses, we see the violent reaction to the helium flash from points five to six. Each doubling back of a star's track corresponds to the ignition of a heavier nuclear fuel. More importantly, we can see that the various luminosity classes are nothing more than various stages of a star's life, and that the stars above the main sequence all have distended atmospheres, i.e. high volumes at low densities. This feature becomes critical when another star is in its proximity, as is the case in a close binary pair.

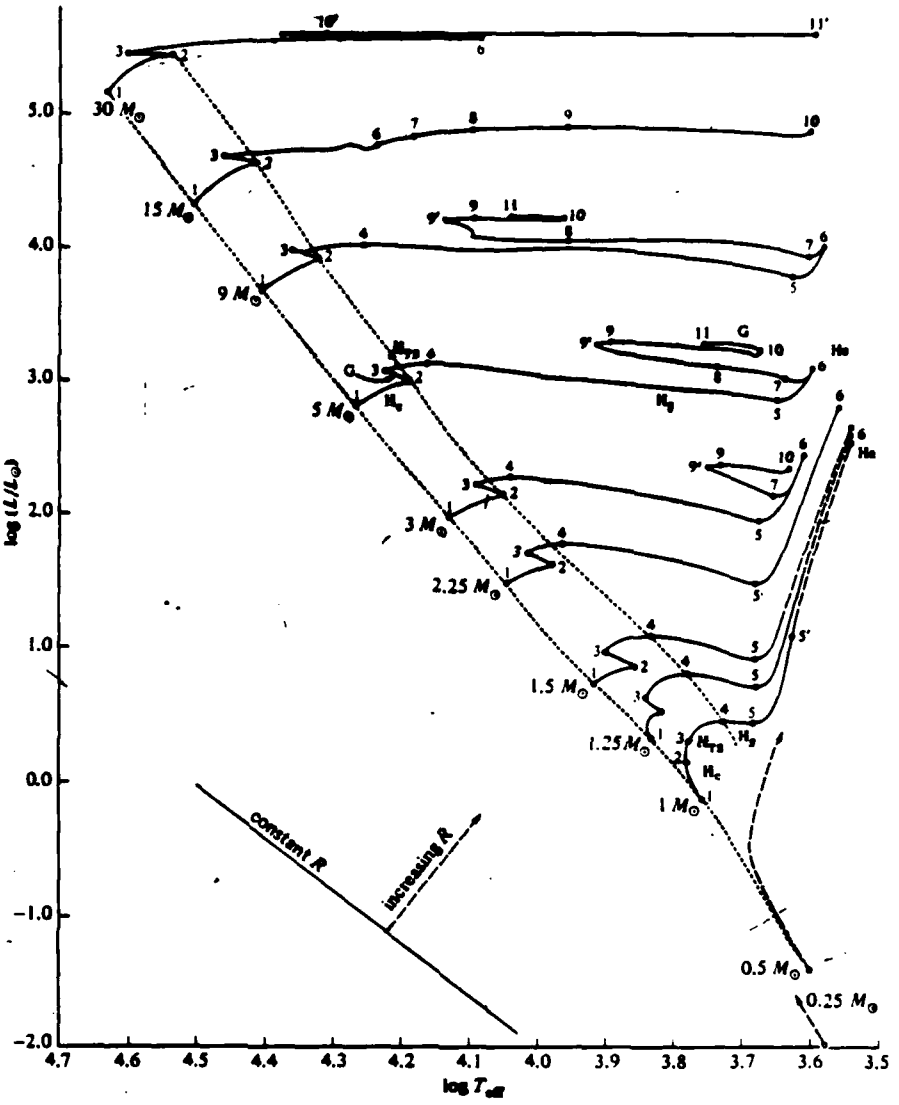


Figure 1-5. Post main sequence evolution on a H-R diagram.

## Binary Systems

We may define a binary system as two stars bound in orbital stability by their mutual gravitation. Binaries which are resolvable as two distinct stars in a telescope are termed visual binaries. Systems which reveal themselves by Doppler shifted spectra (due to the radial component of their orbital velocity) are spectroscopic binaries. Eclipsing binaries, the focus of this paper, betray their presence by periodic changes in their observed light intensity. The eclipsing system holds a special place of importance in astronomy, since they are the most easily discoverable binary type, and binaries are the principal source of stellar masses and absolute dimensions.

Continuing with basic definitions, total eclipse occurs when the larger star completely occults the smaller. The opposite case is annular eclipse. The primary eclipse is the eclipse of greatest reduction in magnitude, and the other, shallower, eclipse is the secondary. The light curve is a plot of intensity against time, which shows the periodic nature of the alternating eclipses, and clearly separates primary from secondary eclipse based on the depth of the minimum.

Three classes of eclipsing binaries can be defined based on characteristics of the light curve. Detached pairs have fairly constant light outside the eclipses and minima of usually unequal depth. Their periods are on the order of several days to years. Semi-detached systems have smoother light curves due to interactions out of eclipse, and also have shallower minima. Their

periods are on the order of days. Contact binaries have very shallow minima of almost equal depth, and eclipses which cover a sizable fraction of the period, which is on the order of a few hours. Figure 1-6[14] shows the relative dimensions of these three types of binaries.

Our task now turns to understanding the mechanisms which vary the light outside eclipses in semi-detached and contact systems. Physical distortion is the simplest of these, and occurs both as tidal distortion due to mutual gravitation, and as equatorial distortion due to the rotation of the star itself. The strong tidal interaction causes both deformation and synchronous orbit, so that the cross-section area radiating towards Earth oscillates with the orbital period. Since the tidal force elongates the

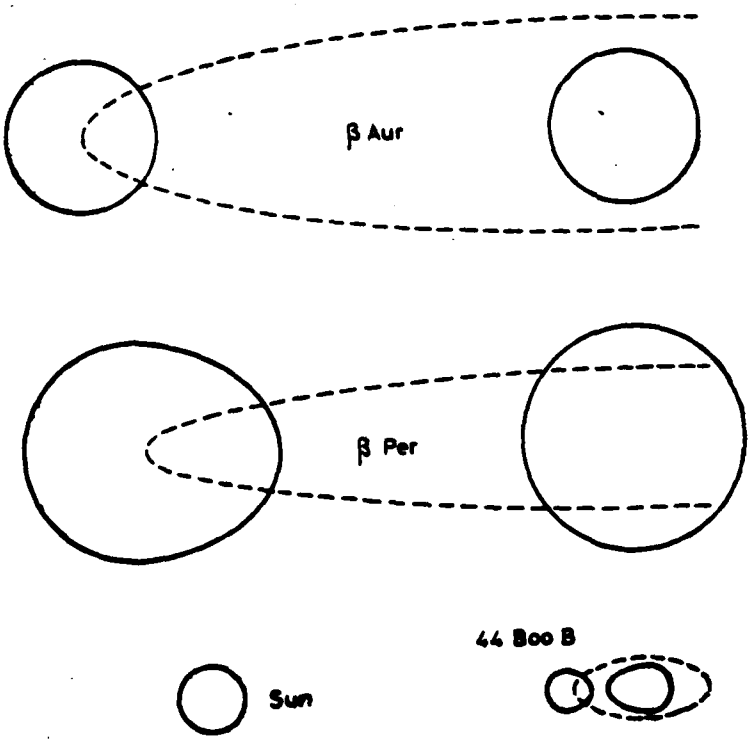


Figure 1-6.

stars along the line joining their centers, this area will be a minimum at eclipse and a maximum a quarter phase later. This tends to distort the entire light curve vertically. The rotational distortion has an effect only when the equatorial planes of the individual components are inclined relative to the orbital plane, in which case the magnitude of this effect should oscillate in sign with the system's precessional period[15], and is negligible on our time scale. Parallel rotational and orbital axes cause the distorted rotating star to always present the same cross-section.

The other major effect on light outside eclipse is the irradiation of one star by the other, sometimes inaccurately called the reflection effect. Radiation falling on one of the stars can be either scattered or re-emitted. In the first case, the temperature of the scatterer is not appreciably raised, and the resultant radiation is partially polarized. In the second case, the temperature of the stellar atmosphere is raised as the incoming photons excite the atoms to various higher energy levels. When these atoms fall back down to lower states, they emit new photons, but not necessarily with the same spectral distribution as before. Both these effects are far too minor to affect the internal state of the star.

The preceeding effects alter the light curve primarily out of eclipse; let us now examine variations in the eclipses themselves. Limb darkening is the most prominent of these. This causes the parts of the surface further away from the observer to appear darker since the stellar atmosphere grows opaque at a higher (cooler) altitude. This also has a color dependency, as

optical depth is a function of wavelength. Limb darkening increases the initial rate of intensity decrease during eclipse, and can suggest a rule for determining which eclipse is total. During totality, we see only the occulting star (constant light) until the smaller star re-appears; but during an annular eclipse, we see the smaller move across the larger. Since limb darkening makes the center of the larger star appear brighter than its edge, we should find a slight "U" during the minimum of the annular eclipse. Thus totality occurs when the minimum is flat.

Gravity darkening affects distorted stars. This varies the emergent intensity proportionally to the local gravitational acceleration[16]. This acts independently of limb darkening; those regions closer to the volumetric center of the star will appear darker than those further away. The orientation of the star can thus make these two darkening mechanisms either reinforce or cancel each other's contribution.

To obtain a more useful classification of binary systems, one which is also better suited for the discussion of binary evolution, we must make use of the Roche model[17]. We envision a co-ordinate frame whose origin is at the system's center of mass and which rotates such that the X-axis always joins the centers of the two stars. The potential U at point (x,y) becomes:

$$U=-GM\left[\frac{1-f}{r_1}+\frac{f}{r_2}+\frac{x^2+y^2}{2a^3}\right] \qquad (1\text{-}5)$$

where: M = the total mass of the two stars
f = the fractonal mass, $m_1/m_2$ such that $f<1$
a = the separation of the two stars
$r_i$ = the distance from star$_i$

Setting U equal to a constant and solving for x and y generates equipotential surfaces as illustrated in Figure 1-7. For large U, the equipotentials are closed ovals about the masses. As U decreases, the ovals grow larger until some $U_{crit}$ where they touch at one point, $L_1$. We call this surface the Roche limit or lobe. Matter at point $L_1$ will be in unstable equilibrium. For U less than $U_{crit}$, both stars are contained within the same equipotential, and they lose their binary nature. We may then think of the Roche limit as the largest closed equipotential capable of containing exactly the whole of each component, as governed by the mass ratio, f.[18]

We can now use the Roche limit as a basis for defining binary types. A detached pair has both components well within their respective lobes. A semi-detached pair has one star filling its lobe, while the other is within its limit. A contact binary has both stars filling their lobes, and can be considered in contact at $L_1$. The shape of the Roche lobes suggests great tidal distortion, but we must realize that only the outer atmosphere is greatly distorted; the compact nuclear burning central region remains unaffected, and evolves as only a function of the star's mass.

To see the importance of Roche lobes to the evolution of a close binary system, consider what happens to an aging star whose outer layers are distending. Since the size of the lobe is determined by the mass ratio and the separation, both of which have no reason to change while the stars are within their lobes, the volume available for expansion is constant and limited. Thus, the

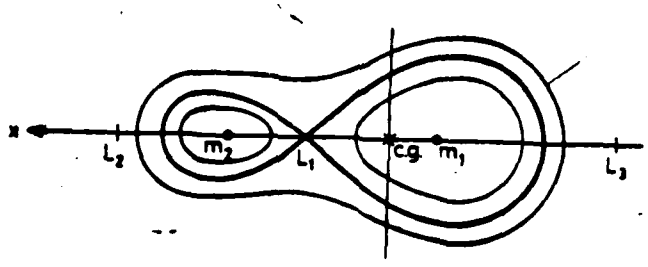


Figure 1-7. Gravitational equipotentials.

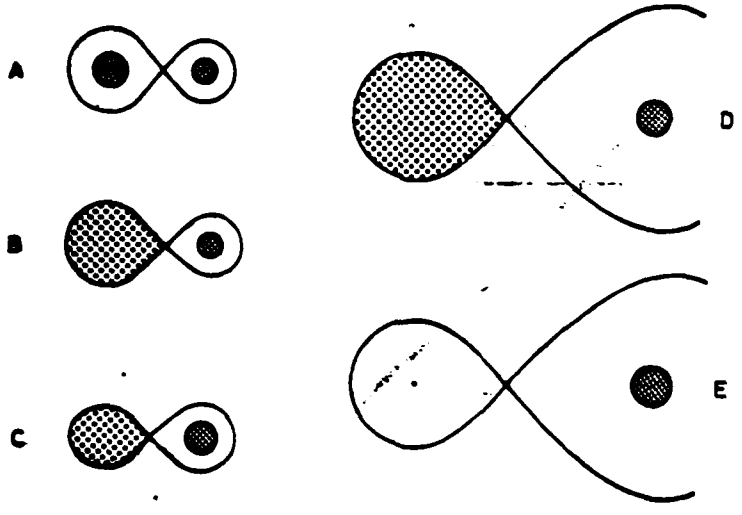


Figure 1-8. Hypothetical mass transfer.

outer layers of one star will eventually distend through $L_1$, and mass will transfer between the two stars. This will in turn change the mass ratio, and thus the size of the lobes. This effect is illustrated (with exaggeration) in Figure 1-8.[19]

Kopal presents a detailed account of the mechanisms of mass transfer.[20] Bypassing the mathematic formalism, he predicts different trajectories for a particle escaping from a star at its Roche limit depending on the particle's ejection velocity. The particle can go to the other star, directly or after orbiting the system; it can return to the original star after passing around the other star one or more times; or it can escape the system altogether. The greater the ejection velocity, the more orbits the particle will make.

Some of these paths end on the star already at its Roche limit. This star cannot stably accept additional matter, thus the flow will increase so that the star remains at its limit. Along with an increase in flow rate comes increased ejection velocities, which leads to more particles in motion around or escaping from the system. This model therefore predicts circumstellar activity in the form of streams or rotating disks. This adds another complication to the light received on Earth.

Turning to the question of binary evolution, we find three basic theories which attempt to explain binary formation. The first proposes that two initially separate stars gravitationally capture each other. However, regions of high stellar density, where such a capture should be more probable, show no signs of an inordinately high percentage of binary systems. The second calls

for the fission of a stellar body into multiple components, but strong density gradients in internal regions of star prohibits such fragmentation.[21]

The third theorizes a pre-stellar fission; the condensation of a contracting cloud about multiple mass centers. For this gravitational instability to occur, the pre-stellar cloud must have more than one-hundred solar masses, and a volume of about a cubic parsec. We can see why there should be fragmentation by examining the cloud's angular momentum. Due to both the large radius and the effects of differential rotation, the collapsing cloud has very high angular momentum, (on the order of $10^7$ times that of a normal star), which limits its contraction as a single body. Yet the cloud wants to reduce its gravitational potential energy as much as possible; to do this while conserving angular momentum, it may fragment into many sub-systems. The angular momentum is conserved by the revolution of the fragments about the total center of mass, and each fragment can individually contract. We are left with a large system, mostly in two to four star sub-systems with stray singlets.[22] All these stars also share similar initial composition since they have a common spawning ground.

Let us now follow the evolution of a hypothetical binary, starting after both components have started nuclear burning, and are both within their Roche lobes. The more massive star will deplete its hydrogen and leave the main sequence first; thus it will also be the first to reach its Roche limit. From the onset of nuclear burning to the time it fills its lobe, the system will be detached. Both components are in the main sequence, although the

primary may be slightly above for a short while, from hydrogen depletion until it fills its lobe.

The primary's expansion will be checked at its Roche limit. With further expansion, it will lose mass to the secondary. If both are still on the main sequence at this point, the transfer will leave the primary the less massive star, the new secondary. The system is now semi-detached with a contact secondary. This is called case A mass transfer, and was depicted in Figure 1-8. If the primary is off the main sequence when it fills its lobe, it will lose its distended outer layers, which have very low density. Thus it loses much volume but little mass; the mass ratio remains about the same, but the secondary's Roche lobe now becomes full. After losing these outer layers, the primary recontracts to within its lobe. This is termed case B mass transfer, and again leads to a contact secondary. Observation bears out this expectation, although there is a chance to observe a contact primary. This is highly improbable, however, since the time spent in the contact secondary configuration is at least two orders of magnitude greater than its transient stay in the contact primary configuration.[23] The contact secondary moves above the main sequence with the characteristics of a subgiant.

The mass transfer leading to semi-detached systems also provides some interesting insights. For example, a system with initially highly unequal masses will, after mass transfer, have a higher, but still low, mass ratio. If multiple transfers occur, each one will raise the mass ratio. This suggests that systems with very low mass ratios are young systems, although we cannot be

certain that systems with high ($f \approx 1$) mass ratios are old, since they may have formed in that state.

Theories concerning contact binaries are much more tenuous. Observations show that these systems have minima of approximately equal depth, implying either equally luminous stars, a masking layer of circumstellar material, or both. Also, in all systems studied for sufficient lengths, the period has decreased consistently, which can be explained by a constant mass loss of about $10^{-7}$ solar masses per year.[24]

Most importantly, contact binaries considerably outnumber all other types. There are two fundamentally different ways of explaining this preponderance. The first asserts that both components have filled their Roche lobes by expansion, have become stable through mass loss across an outer Lagragian (points $L_2$ or $L_3$ in figure 1-7), and remain in an evolutionary trap. Thus contact binaries would represent an old configuration. Observations show, however, a marked absence of contact binaries in globular clusters and other regions of older star population. This effectively casts doubt on this theory of contact formation, unless there is some unspecified outside disrupting force which acts on them in the $10^{10}$ year lifetime of old clusters, or unless the regions of older stars were uncondusive to binary formation.

We can also theorize that contact pairs are young, that they form in or nearly in their present configuration. This easily explains their appearence in young clusters, and is completely independent of any future catastrophes which may cause their absence from older clusters. However, their formation must be an

extremely common event to account for their large numbers. If true, this leads to general predictions concerning the formation of all stars; the contraction of extremely large pre-stellar clouds about multiple mass centers should be the rule rather than the exception.

Regardless of their questionable origin, they do exist and there are some solid physical characteristics of contact pairs. Since both fill their Roche limits, the more massive must also be the largest, but the secondary can be shown to be the brighter. The existence of great tidal forces would ensure an equality in macroscopic features; a system with highly unequal masses would tear itself apart at such close distance. Specific component qualities such as spectral and luminosity class must await observational placement of the H-R diagram, but we would expect both stars to be quite near the main sequence.

This, then, is the theoretical knowledge necessary to interpret the results of this paper, the temperature and luminosity of individual components of binary systems, in terms of binary evolution. The next section will treat the theory behind the actual determination of these quantities from data obtained at the telescope.

## II - Experimental Design

In light of the preceding theoretical considerations, one can infer quite a bit about stellar and binary evolution if one first knows the temperatures and magnitudes (i.e. positions on the H-R diagram) of the components of binary systems. This therefore will be the purpose of this paper: to locate as many individual components of binary systems as possible on the H-R diagram and to investigate the consequences of this plot in terms of binary evolution. To begin, however, we must see how this information is derived, first for the case of a single star, and then for the more complex case of an eclipsing binary.

As we have already seen, the intensity of starlight at two given wavelengths can give a measure of stellar temperature, assuming the light received obeys the Planck distribution. If we introduce a third wavelength (a second color index), we will find that this reading does not necessarily fall on the Planck curve found from the first color index. Clearly, this means that the light received does not conform neatly to a Planck distribution; the third wavelength tells how the star differs from a black body. The second color index is thus a qualitative description of the extra-stellar absorption and the state of the stellar atmosphere; and extremely diffuse atmosphere (as in a giant) will radiate with different absorption and emission peaks than will a normal atmosphere. Together, the two color indices give both the temperature and the luminosity class. This suffices to locate a star on the H-R diagram, without explicitly determining its absolute magnitude.

The use of a standard, well calibrated set of filters greatly facilitates the conversion of intensity levels into temperature and luminosity data. The Johnson and Morgan UBV system[25] was chosen for this purpose. This is a set of three filters: an ultraviolet pass filter centered at 3600Å, a blue pass filter centered at 4250Å, and a visible (yellow-green pass) filter centered at 5350Å. There are many other possible filter systems, but this is the most comprehensively documented, and since it is a broad band system (the three filters have bandwidths of 350Å to 500Å), observation times of dim stars can be kept to a minimum, as more light passes through the filter. Tables for converting UBV data into spectral and luminosity class (temperature and luminosity) can be found in Novotny and Allen.[26]

In order to determine this information for a binary system, it must be eclipsing, and further, it must undergo totality. If we observe the system at totality, we will receive light only from the occulting star, and can easily determine the color indices (B-V) and (U-B) for it. To obtain the same results for the other star, which we never see alone, we must observe the system a quarter phase out of totality, when both stars radiate to us, and then remove the contribution of the known occulting star.

First, let us define the magnitude (at some given wavelength) of both stars together, when the system is out of eclipse:

$$m_b = m_1 \& m_2 \quad , \quad m_2 = m_b \sim m_1$$

where & signifies magnitude addition and ~ signifies magnitude subtraction, both of which are dissimilar to algebraic addition

and subtraction, since magnitude follows a logarithmic arithmetic. To find these operations, we recall (1-2):

$$m_b - m_1 = 2.5\log(\ell_1/\ell_b) \qquad (1\text{-}2)$$

this leads to:

$$\ell_b/\ell_1 = 10^{(m_1-m_b)/2.5} \qquad (2\text{-}1)$$

$$\ell_2 = \ell_b - \ell_1 = \{10^{(m_1-m_b)/2.5}\}\ell_1 - \ell_1 \qquad (2\text{-}2)$$

$$= \{10^{(m_1-m_b)/2.5} - 1\}\ell_1 \qquad (2\text{-}3)$$

thus:

$$\ell_2/\ell_1 = \{10^{(m_1-m_b)/2.5} - 1\} = 10^{(m_1-m_2)/2.5} \qquad (2\text{-}4)$$

Taking logarithms of both sides and simplifying gives:

$$m_2 = m_1 - 2.5\log\{10^{(m_1-m_b)/2.5} - 1\} \qquad (2\text{-}5)$$

which defines $m_b \sim m_1$. Applying this equation to all three wavelengths and taking the proper differences can give us the temperature and luminosity of both components in any binary system which displays totality.

We have yet, however, to correct for the unique calibration of our equipment in relation to the Johnson and Morgan standards, or for the atmospheric extinction which necessarily occurs, especially in such a moist environment as Annapolis. A recently published data reduction method by Harris et. al.[27] was selected for this purpose, primarily because it solves for both instrumental transformation and atmospheric extinction simultaneously, and in the process takes advantage of the Naval Academy's extensive computing facilities. The following argument summarizes this method.

Beginning by treating atmospheric extinction, we define the air mass, X, as the distance through the atmosphere starlight must travel from the star's position to the observer. Geometry shows:

$$X=\sec z(1-.0012\tan^2 z) \qquad (2\text{-}6)$$

$$\sec z=(\sin L\sin\delta+\cos L\cos\delta\cos h)^{-1} \qquad (2\text{-}7)$$

where L is the observer's latitude, $\delta$ is the star's declination, and h is the star's hour angle. This latter quantity is a measure of relative longitude of the star as seen by the observer.

We now assume that the readings outside the atmosphere are related to the measured readings by:

$$(u-b)_m = (u-b)_o + k_{ub}X \qquad (2\text{-}8)$$

The color index (u-b) is solely used in this argument. Any other would develop exactly the same. The extinction coefficient $k_{ub}$ may further be a slightly varying function of color, which we can represent in a truncated power series:

$$k_{ub} = k'_{ub} + k''_{ub}(u-b)_o \qquad (2\text{-}9)$$

Combining:

$$(u-b)_m = (u-b)_o + k'_{ub}X + k''_{ub}(u-b)_oX \qquad (2\text{-}10)$$

Solving (2-10) for the reduced color index gives:

$$(u-b)_o = \frac{(u-b)_m - k'_{ub}X}{1+k''_{ub}X} \qquad (2\text{-}11)$$

Turning to the instrumental transformations, we again write a truncated power series, but this time as a coefficient times the published color index:

$$(u-b)_o = \gamma_1 + \gamma_2(U-B) + \gamma_3(U-B)^2 \qquad (2-12)$$

Combining (2-11) and (2-12) gives:

$$\frac{(u-b)_m - k'_{ub}X}{1 + k''_{ub}X} = \gamma_1 + \gamma_2(U-B) + \gamma_3(U-B)^2 \qquad (2-13)$$

After manipulation and a change of constants:

$$(u-b)_m = c_1 + c_2X + c_3(U-B) + c_4X(U-B) + c_5(U-B)^2 \qquad (2-14)$$

where: $c_1 \equiv \gamma_1$ $\qquad c_2 \equiv k'_{ub} + \gamma_1 k''_{ub}$

$c_3 \equiv \gamma_2$ $\qquad c_4 \equiv \gamma_2 k''_{ub}$

$c_5 \equiv \gamma_3(1+k''_{ub}X)$

Our purpose now is to find the coefficients $c_i$ so that we may transform the $(u-b)_m$ into (U-B). To do this, we employ a set of standard photometric stars for which (U-B) is known.

Next, we generalize this solution (2-14) to accomodate multiple nights observing on the same telescope. Recalling the definitions for the coefficients $c_i$, we see that $c_3$ and $c_5$ remain constant for the same telescope, and $c_4$ can be assumed constant over many nights, since $k''_{ub}$ is both small and slow varying. We rewrite (2-14):

$$R_{jk} = (u-b)_{jk} - \{c_{1k} + c_{2k}X_{jk}\} - \{c_3 + c_4X_{jk}\}(U-B)_j - c_5(U-B)_j^2$$

where $R_{jk}$ is the residuals tensor, ideally zero. The j-index tracks the star out of n total stars, and the k-index tracks the night out of m total nights observing.

We add a weighting factor, as a function of the air mass observed through, to obtain:

$$S = \sum_{k=1}^{m} \sum_{j=1}^{n} \omega_{jk} R_{jk}^2 \qquad (2\text{-}15)$$

which we try to minimize.

We now make another change in variable to write:

$$R_{jk} = (u-b)_{jk} - \sum_{i=1}^{2m+3} g_i Z_{ijk} \qquad (2\text{-}16)$$

where:

| | | |
|---|---|---|
| $g_i = c_{1i}$ | $Z_{ijk} = \delta_i{}^k$ | $(1 \le i \le m)$ |
| $g_i = c_{1(i-m)}$ | $Z_{ijk} = \delta_{i-m}{}^k x_{jk}$ | $(m+1 \le i \le 2m)$ |
| $g_{2m+1} = c_3$ | $Z_{(2m+1)jk} = (U-B)_j$ | |
| $g_{2m+2} = c_4$ | $Z_{(2m+2)jk} = x_{jk}(U-B)_j$ | |
| $g_{2m+3} = c_5$ | $Z_{(2m+3)jk} = (U-B)_j^2$ | |

This allows us to find the minimum of S:

$$\frac{\partial S}{\partial g_p} = 0 = 2 \sum_{k=1}^{m} \sum_{j=1}^{n} \omega_{jk} \left[ (u-b)_{jk} - \sum_{i=1}^{2m+3} h_i Z_{ijk} \right] \frac{\partial \sum h_i Z_{ijk}}{\partial g_p} \qquad (2\text{-}17)$$

$$0 = \sum_{k=1}^{m} \sum_{j=1}^{n} \omega_{jk} \left[ (u-b)_{jk} - \sum_{i=1}^{2m+3} h_i Z_{ijk} \right] Z_{pjk} \qquad (2\text{-}18)$$

$$\sum_{kj} \omega_{jk} (u-b)_{jk} Z_{pjk} = \sum_{ikj} h_i \omega_{jk} Z_{ijk} Z_{pjk} \qquad (2\text{-}19)$$

For ease if notation, let us here shift to tensor notation, defining:

$$\begin{aligned} G_\mu &\equiv g_i \\ S_\sigma \equiv s_p &= \sum\sum \omega_{jk} (u-b)_{jk} Z_{pjk} \\ Z_{\mu\sigma} \equiv z_{ip} &= \sum\sum\sum \omega_{jk} Z_{ijk} Z_{pjk} \end{aligned} \qquad (2\text{-}20)$$

Thus finally,

$$S_\sigma = Z_{\sigma\mu} G_\mu \qquad (2\text{-}21)$$

or, since the coefficients we seek are contained in $G_\mu$,

$$G_\mu = Z_{\mu\sigma}^{-1} S_\sigma \qquad (2\text{-}22)$$

At this point, since the dimensions of these tensors are more than twice the number of nights observed, the power of large digital computers becomes attractive. Appendix II shows the programs used to calculate $G_\mu$ from the observed data. Once we have $G_\mu$, we can re-enter equation (2-14) to find (U-B) for an unknown star observed on some night k.

The advantages of this method primarily lie in the increased ease and flexibility it gives the observations themselves. First, since all standards observed affect all coefficients, an error in any one will be more effectively compensated by the others. Further, since the quality of the final results depends on the total number of standards observed, the observer is not forced to study any given standard at any given time, allowing for capricious weather patterns. Similarly, nights of poorer optical quality can still be of some use by giving them a lower weight.

We are now armed with all the theoretical weaponry needed to convert raw data into a real measure of temperature and luminosity for the individual components of a binary system. Any modification of these techniques will arise through peculiarities of the equipment itself. Let us now describe this equipment and its effect on the data taking process.

Clearly, the single most important tool for astronomical research is the telescope, used not to magnify, but to gather as much light as possible. The Naval Academy's telescope is a Ferson Optics 1216, a sixteen inch reflector, located on the roof of Michelson Hall. The telescope has console and remote control of the coordinate slew motors (both slow and fast), the cassegrain focus, and the observatory dome. With the photometer head attached at the cassegrain focus, the telescope has a focal ratio of 14:1.

The only important operational deficiency of this instrument was the inability of the sidereal drive system (which should compensate for the rotation of the Earth) to track a star for periods greater than a minute, especially when the telescope was positioned far from the vertical or when the ambient temperature was either cold or quickly changing. Proper balancing minimized this problem, but it was still everpresent. Fortunately, however, observational procedure could be altered so that data taking become insensitive to telescope drift, albeit more time consuming.

The core of the observational equipment was the Thorn EMI Gemcon Starlight 1 stellar photometer. This photometer consists of two fundamental parts, the photometer head and a digital counter. The photometer head was attached at the cassagrain focus of the telescope, and steadied against rotational and axial displacements by a metal plate fixed fast to the telescope and attached to the head by four long bolts. The head was further secured in a sleeve extending from the telescope by three set screws.

The purpose of the photometer head is to detect light through the telescope and to convert it into a useful electrical signal. Diaphragm and filter turrets, a photomultiplier tube, and a power supply constitute its major components. The diaphragm turret allows one to select one of five aperture sizes, ranging from .01" to .199". Each position has two stops: one sets the aperture in the center of the field of view, for observing the star under study, and the other slightly offsets the aperture to give sky background measurements while still maintaining the track on the star. This feature saved considerable amounts of time and increased the reliability of the results through the added consistency it gave the observations.

The filter turret operates in a similar manner to allow selection of a specific filter. The filters supplied in the photometer head are as follows: ultra-violet, 1mm. Shott UG-1; blue, 1mm. Shott BG-25; and visible, 1mm. Shott OG-515. These are the filters most compatible with the supplied photomultiplier tube. The filter turret also has two empty positions for other filters if desired, which were not used, and an opaque filter to protect the photomultiplier from ambient light when not in use.

The photomultiplier tube supplied is the EMI 9924A, which is ideally suited to UBV photometry. Its spectral range is from 3100Å to 6700Å, with peak response at 4200Å. This tube also does not need to be cooled to give good results, so that the set up of the equipment was much simpler and faster. The dark count of the tube (the intrinsic background noise) ranged from about seventy counts per second at $0^{o}C$ to ninety cps at $20^{o}C$.

The counter receives the output signal from the photometer and displays a number on its LED digital readout. The obvious advantage of a digital counter over the usual strip chart recorder is the higher precision achievable for low light levels. The maximum light count before counter overflow is $10^8$, which was never reached in any observation. The counter also has several sophisticated capabilities, such as interface with other photometer heads or with a microcomputer, none of which were needed nor utilized.

The counter may be operated in two modes. It starts on command from the observer, but may stop either after a pre-determined time (.01, .1, 1, or 10 seconds), or when the observer himself stops the count manually. The first mode was used throughout, with a count time of one second. This time was selected over a longer one as a compromise between poor telescope tracking, as previously discussed, the desire to keep the aperture size to a minimum, usually .02" or .0313", and better statistical behavior of longer count times.

A correction must also be made for pulses too close for the electronics to resolve as distinct. This "dead time" is calculated by plotting log(n) against magnitude for some dim stars of known magnitude, where n is the displayed count. This should result in a straight line. A bright star is then observed, and when plotted, will be below this line. The dead time is:

$$d = (N-n)/n^2 \qquad (2\text{-}23)$$

where N is the count predicted be the plot. The corrected count

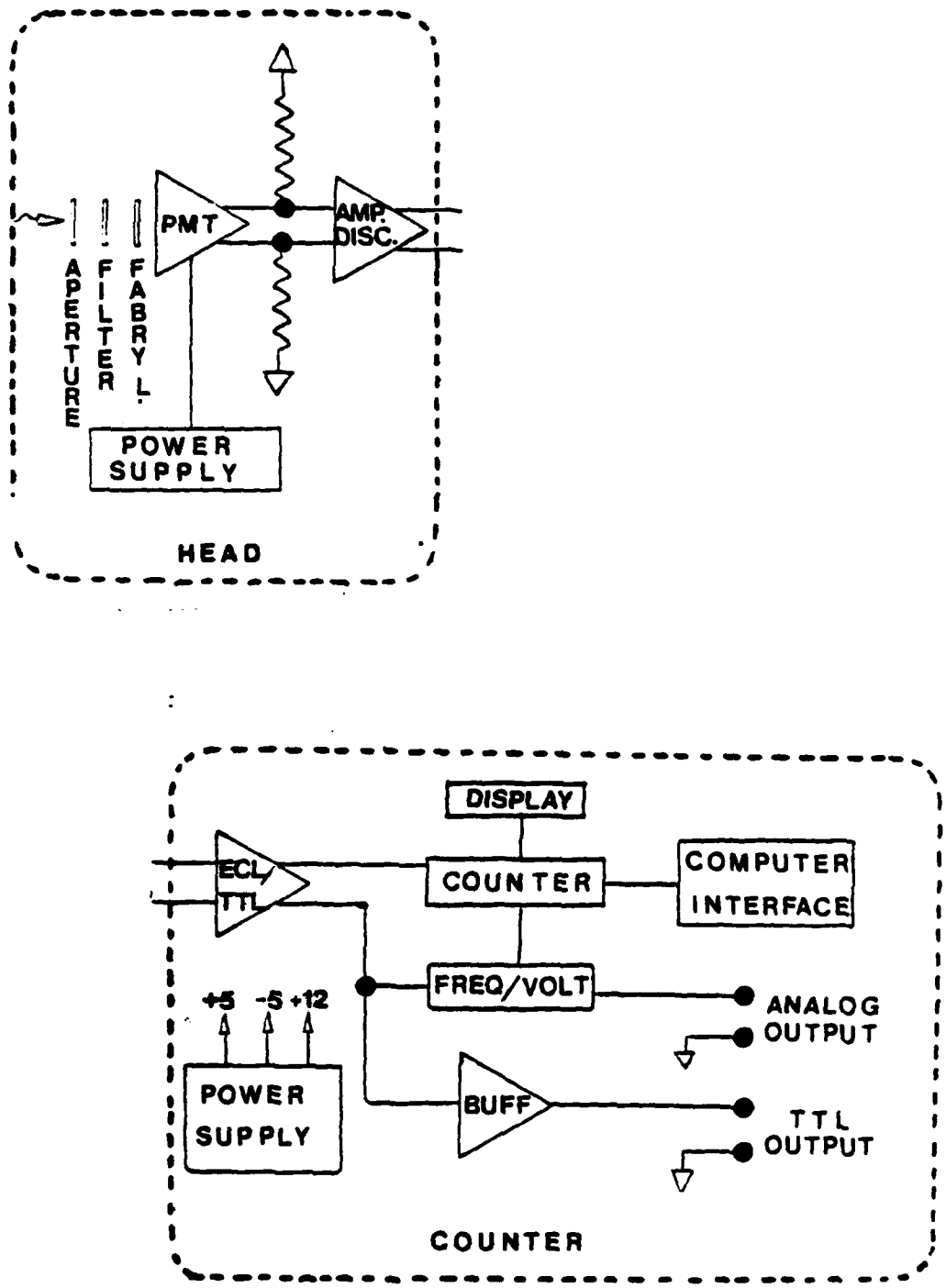


Figure 2-1. Schematics of the photometer head and counter.

now becomes:

$$N = n(1+dn) \qquad (2\text{-}24)$$

For our tube, the dead time was calculated as 100nsec. We can see that this is a very small correction for all but the standards and the brighter of the eclipsing binaries.

Figure 2-1 shows the path of a hypothetical photon as it enters the photometer head. The photon first encounters a flip prism, which is controlled by the observer to either view the star or to measure its intensity. Notice that it is before the filter in the optical path, so that one can see and track the dimmest stars without light loss through the filters. The prism, in the view position, also provides a safeguard against photomultiplier damage due to ambient light.

Having this equipment, we now need specific stars to observe with it. For this project, two sets of stars are required: one set of eclipsing binary systems for which temperature-luminosity data are as yet unknown, and another of standard stars with known color indices, which control the generation of the reduction tensors discussed previously. A list of unknown eclipsing systems was provided by Dr. Richard L. Walker[28] of the U.S. Naval Observatory, Flagstaff Station. His original list consisted of some eighty systems brighter than twelfth magnitude, with a good spread in right ascension. The first condition arises as a practical limit of local visibility, a function of both our equipment and local observing conditions. The second condition ensures that there will be something to observe regardless of the time of the year.

A list of standard stars was compiled by the author from the list of UBV standards given in Johnson and Morgan.[29] Standards were selected with two criteria: to ensure that their co-ordinate distribution followed that of the program stars, minimizing undetected positional variation in extinction; and to ensure a spectral and luminosity class distribution similar to one expected for components of eclipsing binaries of any type, minimizing undetected variation in instrumental transformation.

Since the beginning of the project, the list of unknown systems has undergone several revisions for a variety of reasons. The most common of these was too long a period for our time frame. The maximum period was arbitrarily set at thirty days. To illustrate the rationale of this choice, consider that not quite one night in seven was of observable quality. Unobservability can arise from many causes: a cloud cover, a bright moon, etc. It is a landmark frustration of astronomical research that one cannot control the laboratory; one can only entreat the Aesir and hope for clear nights. If a system eclipses once each month, then on the average we can see only one every seven months. Take into account also that in this time, the Earth would precess through more than twelve hours in ascension, and that there is no guarantee that the eclipse will occur during hours of local darkness; it clearly becomes more time efficient not to bother with long period systems, but to concentrate on completing others with shorter periods.

To observe an eclipsing system in totality, other information

is also required. One must know the system's ephemeris, its schedule of primary eclipses. Ephemerides were found in several sources, primarily Koch[30] and Rafert.[31] If a system's ephemeris has not been determined, however, we cannot use it since the time of totality is unknown. The amount of time required to calculate an ephemeris observationally, especially with the capricious nature of local weather conditions, would be prohibitive to completing the initial purpose of the project.

One must also be able to locate the system in order to observe it. Co-ordinates for all the systems were found in Kurkarkin[32] for 1 January 1900. These were precessed to 1 January 1983 for observational purposes and to 1 January 1950 for reference to the Smithsonian Astrophysical Observatory Star Atlas[33] in order to prepare finder charts. The method of precession used was the programmable calculator method of Shudde.[34] Three systems were not found on the SAO atlas.

However, the most limiting factor governing which systems were observable was nothing so subtle as the above, but rather that the photometer system, which was ordered in April, did not arrive until mid-January. Adapting the telescope mountings to compatibility with the photometer head and initial testing tied up the equipment until late January. Appendix III lists the observable systems from Dr. Walker's list, their co-ordinates, period, maximum hour angle to allow an air mass $X<1.5$ (as recommended by Harris[35]), and the number of totalities exhibited in local hours of darkness within $h=\pm h_{max}$ between the date of equipment readiness and the end of April. One can easily see that there are several

systems completely unobservable and that only about a dozen have a better than fifty-fifty chance of showing just one totality, given a one in six "good night" ratio.

Although this severely limits the statistical nature of the results, accuracy can still be expected if observations are done such that each is statistically valid. To this end, observation of any event consisted of at least ten one-second counts per filter, and a standard star, preferably one near the unknown system, was observed immediately before and after. Also, somewhat paradoxically, this forced the decision concerning the acceptibility of observing conditions to become more discriminative; more than one observation has been ruined by nothing more than a small, stray cirrus cloud.

## III - GENERATION OF RESULTS

The most useful illustration of the method by which values of component temperature and luminosity are obtained would be to take a specific system and trace the procedure step by step to completion. For this purpose, let us choose W Ursae Majoris, the first system for which a solution was obtained. The co-ordinates of this system are: 9h42m34s in right ascension and $56^{\circ}01'49"$ in declination. Its maximum visual magnitude ($m_b$) is +8.5, and its magnitude in totality ($m_l$) is +9.2.

The first step is to calculate a schedule of total eclipses for the system. Its ephemeris is:

$$2,434,489.44286 + .3336384E \qquad (3\text{-}1)$$

The first term is a fixed time, an epoch, expressed in the astronomical system of Julian dates, and the second term is the period, in days, multiplied by an integral number of eclipses (E) to show periodicity.

The computer program (see Appendix II) written to print out a schedule of observable events uses the first totality in October 1982 as a starting point. For this ephemeris, this is 02:33:50 EST 1 October. The program then prints all events for this ephemeris between 20h00 and 04h00 (local hours of darkness), assuming circular orbits, so that totality and quadrature are one-quarter period apart. The effect of this assumption is quite valid, even if the assumption itself is not, since the stars are out of eclipse for at least a sixth of a period before re-eclipsing. Tidal forces in systems as close as those to be studied would easily

have absorbed any eccentricities as large as this.

There are still two possible downfalls to the computer-generated event schedule. The first is simply drift in the event times caused by round-off error in the computer. This is easily avoided by using double-precision arithmetic, accurate to twelve decimal places. The second arises because the ephemeris schedules primary eclipse, whereas we are interested only in total eclipses. Along with his list, however, Dr. Walker also indicated what kind of eclipse the primary was, either annular or occulting (total). If the primary eclipse is annular, one just adds half a period to the ephemeris epoch, and uses this time as a starting point for the program. If the primary eclipse is total, this step is not needed. The program outputs the time (in EST) of an event and its corresponding sidereal time. This is a time reckoned by prime meridian passage of the fixed stars rather than the sun, and is entirely local (no system of time zones). Sidereal time allows the calculation of hour angle:

$$h = ST - \alpha \qquad (3\text{-}2)$$

If our sidereal time and a star's right ascension are equivalent, then there is zero hour angle, and the star is on our meridian.

We now recall Harris' previously discussed caveat of limiting the maximum air mass to $X<1.5$. This becomes especially important considering the nature of this project; since we have a very limited number of observations per system, the accuracy of each becomes exceedingly crucial. From equation (2-6), the air mass is a function of only the observer's latitude, and the star's declination

and hour angle. The latitude is fixed for all observations at $38^{o}58'$, and for a given star, declination is also constant. Thus to limit the air mass, we must limit the hour angle. Solving (2-6) first in terms of cosz for h=1.5:

$$\cos^2 z(.9988-1.5\cos z) = .0012 \qquad (3-3)$$

Then in terms of cosh:

$$\cosh_{max} = \frac{\cos z - \sin L \sin\delta}{\cos L \cos\delta} \qquad (3-4)$$

This uniquely determines a maximum hour angle, and events whose hour angle is greater than this are scratched from the schedule.

The next step is to observe events on our revised schedule. The system is sighted by use of the finder telescopes by comparing stellar field patterns to the finder chart. This step was the most surprisingly difficult of the entire observational procedure, since star fields never quite seemed to agree exactly with those published on the SAO atlas. Once the system is located, it is centered in the smallest aperture which allows moderately good tracking, (the star remains in the aperture for at least half a minute). At least ten readings are made for each filter in the following sequence: system observation in V, background count in V, system and background in B, then both in U. Albeit lengthier because of increased setting changes, this cycle gives more accurate results than other possibilities, such as taking all V counts at once, since time-dependent errors (turbulence or sparse stratus clouds) will be spread evenly over all wavelenghts, minimizing uncompensated error in any one. The readings for the system

and its background at each wavelength are then averaged, and are corrected for instrumental dead time (2-24). The corrected background count is now subtracted from the corrected system count to give the contribution of just the system itself: $n_v$, $n_b$, $n_u$. Color indices are then computed via:

$$(b-v) = -2.5\log n_v/n_b \qquad (3-5)$$

here using (b-v) as an example.

Before discussing the reduction of the observations of the program stars, let us digress to the generation of the reduction tensors used in Harris' method. Observational data of standard stars is fed into the computer (see Appendix IV), which calculates $G_\mu$ in the sequence shown in Figure 3-1. It is important to note here the precision of the inversion of $Z_{\mu\sigma}$; the accuracy of $G_\mu$, and thus the validity of the entire set of results is at the mercy of this single operation.

With $G_\mu$, we are ready to find the actual color indices of the system. Equation (3-6) is the governing relation for this process:

$$0 = (b-v) - g_{1k} - g_{2k}X_k - (g_3 + g_4X_k)(B-V) - g_5(B-V)^2 \qquad (3-6)$$

This is exactly equation (2-16), but with the residuals tensor, $R_{jk}$, set equal to zero. Taking the proper elements of $G_\mu$, it is a simple matter to calculate the actual color index, (B-V).

To find the proper elements of $G_\mu$, we recall its theoretical derivation (2-20). $G_\mu$ has 2m+3 elements, where m is the total number of nights observed. The night of the specific observation

```
*OLD YLEYN
######## <-- "YLEYN" password
*RUN BASIC7
INPUT # OF NIGHTS, # OF STARS? 10,12
INPUT 1 FOR (B-V), 2 FOR (U-B), 3 FOR V-V? 2

*OLD TENSOP
######## <-- "TENSOP" password
*RUN
INPUT # OF NIGHTS? 10
DOEST THOU WISH TO SEE Z AND S? NAY

DOEST THOU WISH TO SEE Z(-1)? NAY

DOEST THOU WISH THE ACCURACY OF Z(-1) CONFIRMED? VERILY
 2.77703E-2 IS THE SUM OF TOTAL ABSOLUTE DEVIATION OF Z*Z(-1)
  FROM THE IDENTITY TENSOR.

DOEST THOU WISH TO SEE Z*Z(-1)? NAY

*** FIAT G ***

 0.983246
 0.188366
 0.793835
-3.17451
-1.00731
 1.07757
 3.78274
 1.48077
 3.90839
 1.22079
 0.651284
 1.46009
 0.933666
 4.71509
 2.6865
 0.591152
-1.93425
 0.187146
-2.00736
 0.312506
 1.6225
-0.520144
-7.81229E-2

*
```

Figure 3-1. Generation of the G tensor.

sets k; thus $g_{1k}$ is the $k^{th}$ element, $g_{2k}$ is the $(m+k)^{th}$ element, and $g_3$, $g_4$, and $g_5$ are the last three elements. As an aside, we can see that truncating our power series (2-9),(2-12) was indeed justified by the small co-efficient $g_5$.

Inserting the data for W Ursae Majoris into (3-6) gives the following results:

$$\begin{aligned} (B-V)_b &= .590 \qquad (B-V)_1 = .584 \\ (U-B)_b &= .108 \qquad (U-B)_1 = .175 \end{aligned} \tag{3-7}$$

The tables in Novotny[37] use (U-V) as an entering index, which is easily calculated:

$$\therefore \qquad (U-V) = (U-B) + (B-V) \tag{3-8}$$

We can immediately find the spectral and luminosity class of the occulting star, which will locate it on the H-R diagram, by using the forementioned tables.

To determine this information for the second star requires more work. We must subtract the contribution of the occulting star from the measurements made outside eclipse, but we must do this via (2-5):

$$m_2 = m_1 - 2.5\log\{10^{(m_1-m_b)/2.5} - 1\} \tag{2-5}$$

Since a color index is merely the difference in magnitude at two different wavelengths, we adapt this to:

$$\begin{aligned} (b-v)_2 = b_1 &- 2.5\log\{10^{(b_1-b_b)/2.5} - 1\} \\ &- v_1 + 2.5\log\{10^{(v_1-v_b)/2.5} - 1\} \end{aligned} \tag{3-9}$$

$$(b-v)_2 = (b-v)_1 + 2.5\log\left[\frac{10^{(v_1-v_b)/2.5} - 1}{10^{(b_1-b_b)/2.5} - 1}\right] \qquad (3\text{-}10)$$

Equation (3-10) is in the proper form, but to use it, we need a system of maginitudes. We could use:

$$v = -2.5\log n_v \qquad (3\text{-}11)$$

where $n_v$ is the count in the visible band. This, however, in no way accounts for variations in observing conditions among nights, or any other of the possible effects on any single observation. The form of (3-11) is still valid; but we must first normalize our counts.

First, we take $n_{v_b}$, the visible count of the system out of eclipse. We then assign $n_{b_b}$ and $n_{u_b}$ by the relation:

$$n_{v_b} = 10^{(b-v)_b/2.5} n_{b_b} \qquad (3\text{-}12)$$

where $(b-v)_b$ is the result of applying (3-6), given the indices (3-7).

To assign counts for the occulting star alone, we first find the brightness of it in terms of the brightness of both:

$$n_{v_1}/n_{v_b} = \ell_{v_1}/\ell_{v_b} = 10^{(m_1-m_b)/2.5} \qquad (3\text{-}13)$$

We would expect, that if the occulting star is one-half as bright as both stars together, it would have half as many counts. Visual magnitudes for the systems were found primarily in Koch. Once we define $n_{v_1}$, the others are found by again using (3-12). For W Ursae Majoris, these counts are listed below:

$$n_{v_b} = 4349 \qquad n_{v_1} = 2282$$
$$n_{b_b} = 2526 \qquad n_{b_1} = 1333 \qquad (3\text{-}14)$$
$$n_{u_b} = 2287 \qquad n_{u_1} = 1134$$

To obtain a consistent magnitude system, we take the logarithms of these normalized counts, but we can dispense with the factor of 2.5, since it also appears in the denominator of the exponent of (3-10). For W Ursae Majoris, (3-10) gives:

$$(B\text{-}V)_2 = .597 \qquad (U\text{-}V)_2 = .657 \qquad (3\text{-}15)$$

Before entering the tables with the values in (3-7) and (3-15), let us comment on the statistical inaccuracy of Harris' method, introduced by setting $R_{jk}$ to zero. This is the case for the aggregate of standard star data, but is not necessarily true for an individual star. Using standard stars as though they were unknowns, (3-6) gives results that are slightly off the published color indices. However, we can use (B-V) and (U-V) independently to obtain temperature and luminosity, and then assign these two pairs of values as the endpoints of an uncertainty bar. In this way, we can have a graphical measure of the precision of the results without having to subjectively assign error bars based on the behavior of the standard stars.

For W Ursae Majoris, the tables tell us that both stars are F9V stars. The secondary's locus on the H-R diagram runs from (-3.776,0.3) to (-3.775,0.22) in co-ordinates of (-log $T_{eff}$,log $L/L_o$). The locus of the primary is (-3.778,0.065) to (-3.789,0.10). We can see that these results are at least reasonable; the system's period suggests that it is a contact binary, which is supported by

the postions of its components on the H-R diagram, recalling the expectations for a contact pair from the first section.

The alert reader will have noticed that we have not mentioned the light varying effects also discussed in the first section. A quick examination of these will show why they can be ignored. Most importantly, since we observe the system only at two instants, totality and quadrature, their time dependence becomes irrelevant. Distortion now only makes the occulting star radiate to us through a smaller cross-sectional area, and makes the stars at quadrature radiate through a greater area. However, the resulting differences in instantaneous brightness is already taken into account in the measured visual magnitude of the system in and out of eclipse, as found in Koch.

We can dismiss much of the complications of darkening mechanisms by a similar argument. Since we observe only at totality and quadrature, we never see one star crossing the limb of the other, where the darkening mechanisms have their greatest effect on the light curve. Specifically, in the quasi-static limit, limb darkening would make both stars appear slightly cooler than they really are, both in and out of eclipse. Gravity darkening will make the occulting star cooler and dimmer yet in totality, but will make both stars appear relatively brighter out of eclipse. Thus the overall effect would be a solution for the occulting star slightly too cool and dim, and since limb and gravity darkening offset each other at quadrature, the solution for the other component would be slightly too warm. These, however, are insignifigant compared to the uncertainties discussed above.

The irradiation effect is completely irrelevant at totality, since all reflected or re-emitted light travels away from us. Out of eclipse, there will be an irradiation effect, but we will assume that it is also a negligible factor, as Dr. Walker recommends,[38] in order to process as much data as possible. The slight increase in accuracy would not merit the greatly increased time required to reduce this effect, which, like the darkening mechanisms, would lie well within the uncertainty bars.

We have now gained all the information which we set out to determine for this system; we know the spectral class of each component, which gives a measure of temperature. More importantly, the position of each component on the H-R diagram, which gives clues to the evolutionary process in binaries. The procedure outlined above can be used to obtain the same information for any eclipsing binary system exhibiting totality. The next section will highlight the important points of this procedure for the systems observed, display the results graphically on H-R diagrams, and discuss the signifigance of these plots.

# IV - DATA AND INTERPRETATION

The data taken for any event consists of about sixty intensity measurements (ten readings over three filters at two settings each) and an average time of observation. The value of presenting this information in this format is questionable at best, as it would serve only to engulf the reader in unnecessary detail. One would become detached from the more important process of generating the final results.

To keep this sense of flow in the data analysis, values used in key stages of the result generation algorithm discussed in the preceding section will be given for all systems observed. The data page for a system will therefore begin with basic information about the system, coordinates and the ephemeris used. Observational data, after being corrected for instrumental dead time, will then be given, followed immediately by the resultant reduced color indices. As an intermediate step in the calculation of the indices of the occulted star, the normalized counts will also be given. Finally, once we know the indices for both components, their spectral and luminosity classes will be given. An H-R diagram showing the positions of the components will immediately follow each system's data page.

The main sequence on each of these diagrams is the locus of points for the luminosity class V stars from the tables in Novotny. The three diagrams immediately following illustrate various features of this main sequence. The first shows the specific points from the table which define the main sequence. Because

we are dealing with discrete points, the band is not smooth. This will become more evident later. The second plots the sun, primarily to be used as a reference for future diagrams. Already familiar with the characteristics of the sun, we can gain a idea of the physical states of the components in an unkown system by comparing their locations to the sun's. The third H-R diagram is an expansion of the second about the area near the sun. This clearly shows the jaggedness of our main sequence. This plot points out another of its shortcomings. The sun we know to be on the main sequence, but on this plot, it is not. This is because we have represented a band by a line. The reader whose aesthetic balance is upset by these inaccuracies may mentally broaden and smooth the line representing the main sequence on the diagrams. However, since the same line is used in all plots, this is not a critical point.

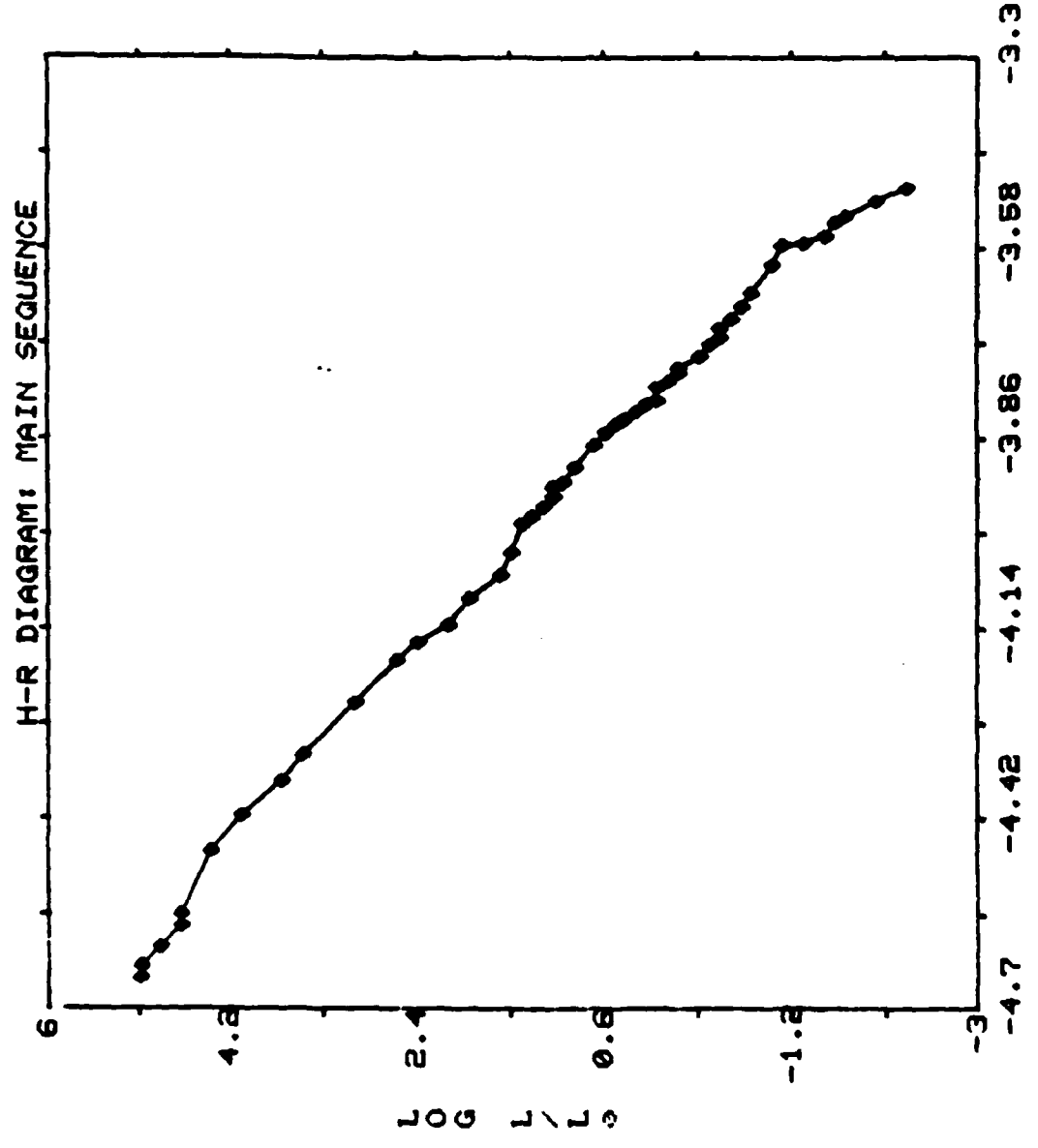
H-R DIAGRAM: MAIN SEQUENCE
LOG L/L⊙
6
4.8
2.4
0.0
-1.2
-3
-4.7
-4.42
-4.14
-3.86
-3.58
-3.3
-LOG Teff

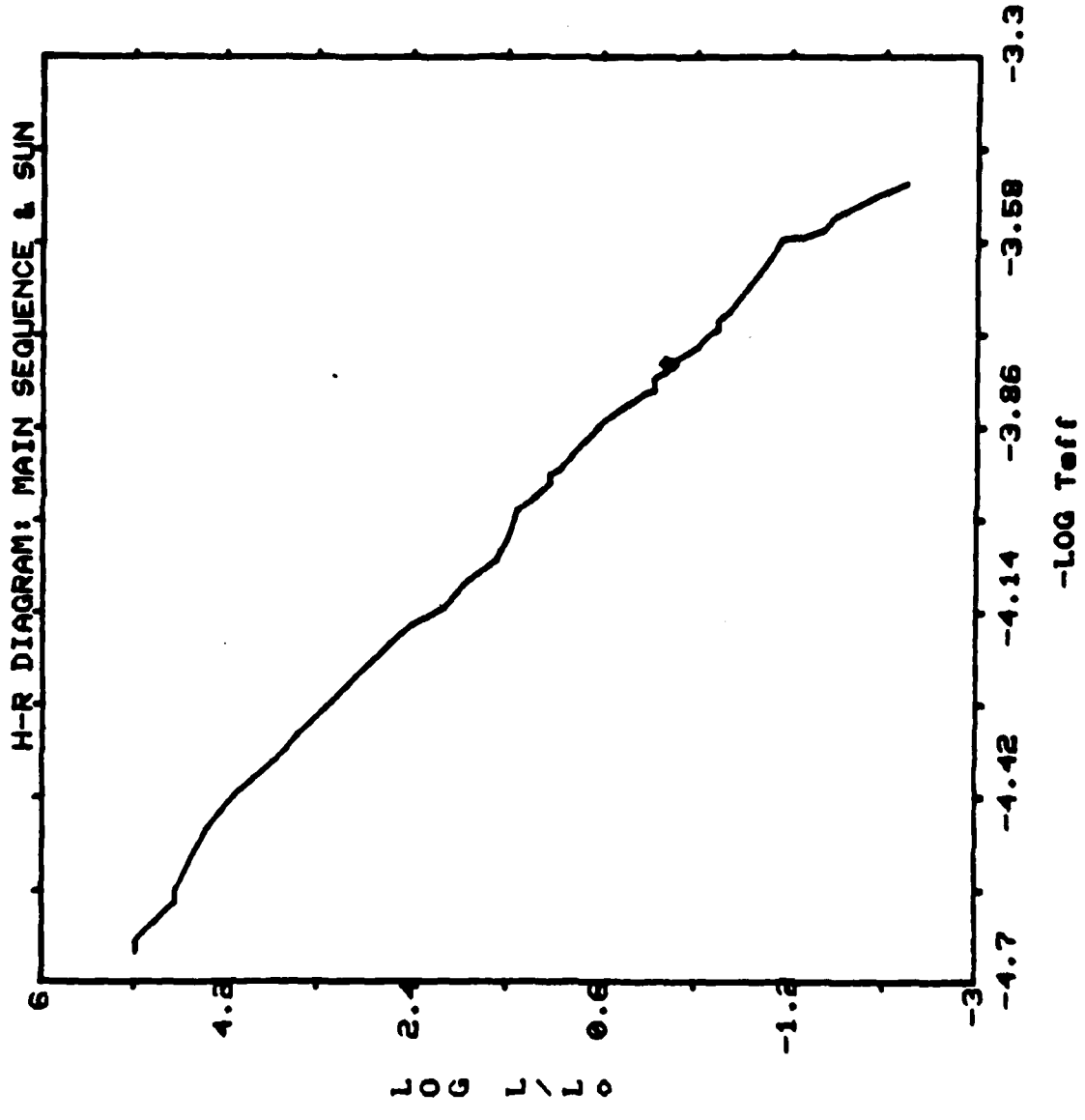
H-R DIAGRAM: MAIN SEQUENCE & SUN
LOG L/Lo
6
4.8
2.4
0.6
-1.2
-3
-4.7
-4.42
-4.14
-3.86
-3.58
-3.3
-LOG Teff

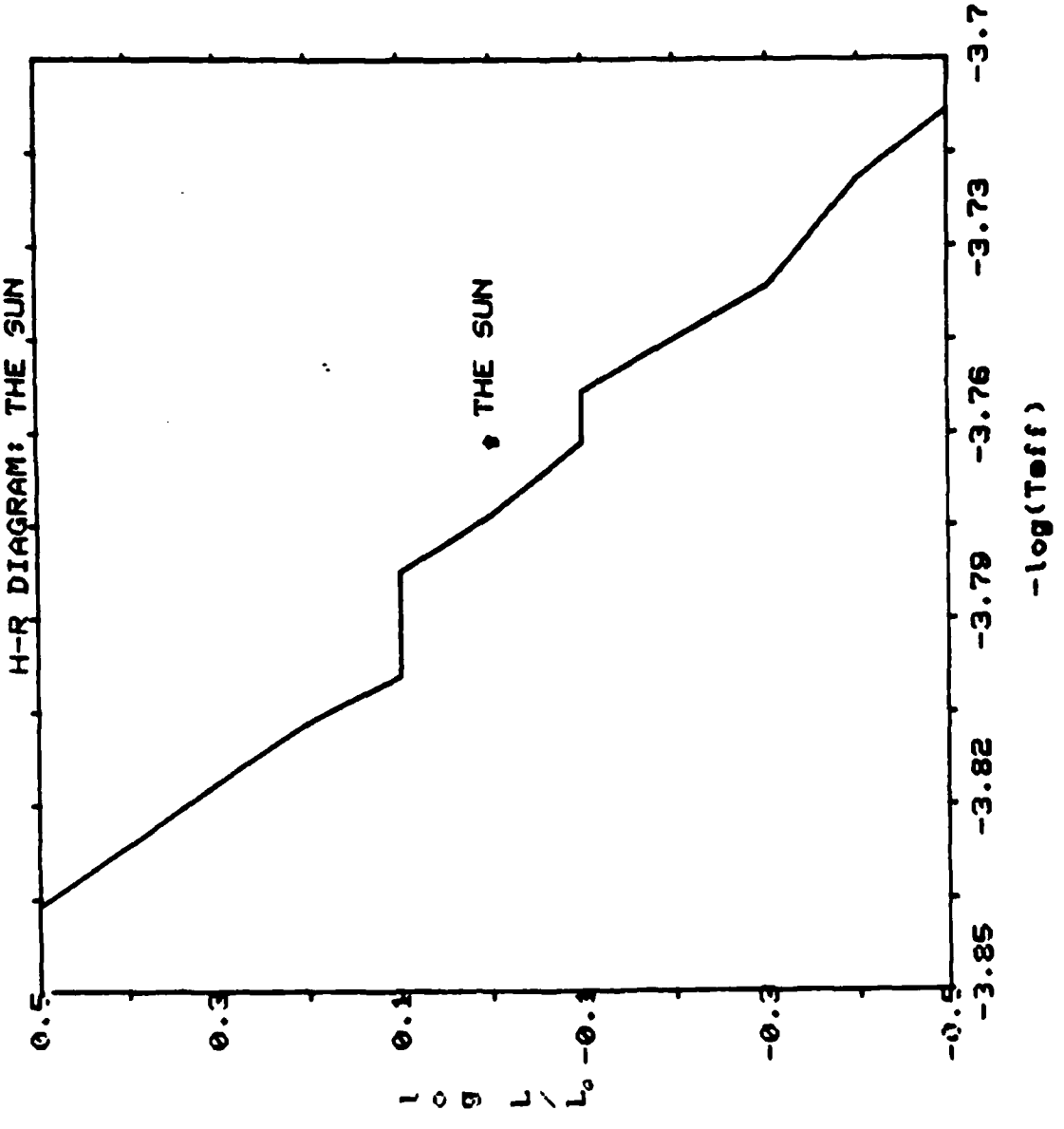
H-R DIAGRAM: THE SUN
THE SUN
0.5
0.3
0.1
-0.1
-0.3
-0.5
log L/L₀
-3.7
-3.73
-3.76
-3.79
-3.82
-3.85
-log(Teff)

# TU CAMELOPARDI

$\alpha$ = 5h53m26s  $\delta = 59^{o}53'09"$

Ephem: 2432633.6555 + 2.933229E

Primary Eclipse = Annular

| | | X | V | B | U | (b-v) | (u-b) |
|---|---|---|---|---|---|---|---|
| Totality: | 4 Apr | 1.211 | 37742 | 34285 | 6713 | .10 | 1.77 |
| Out: | 2 Mar | 1.077 | 48822 | 42313 | 8777 | .16 | 1.71 |

Reduced Color Indices:

$(B-V)_b = .073$  $(B-V)_1 = -.004$

$(U-V)_b = .059$  $(U-V)_1 = .022$

$m_b = 5.5$  $m_{tot} = 5.6$

Normalized Counts:

$V_b = 48822$  $V_1 = 44526$

$B_b = 45647$  $B_1 = 44690$

$U_b = 46240$  $U_1 = 43633$

New Color Indices: $(B-V)_2 = 1.544$  $(U-V)_2 = 2.14$

Spectral Classes: Primary - A1V
Secondary - K4IV

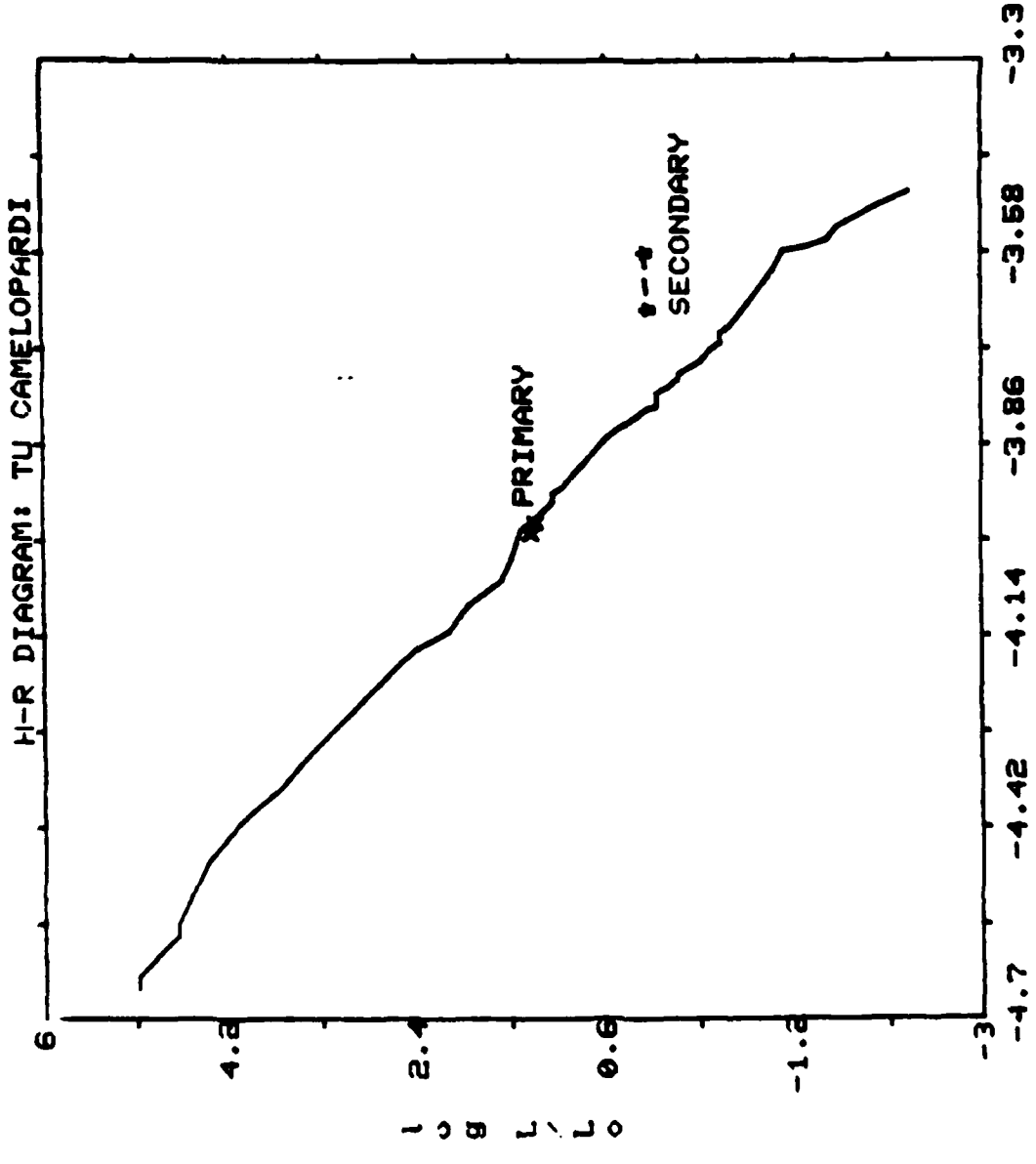
H-R DIAGRAM: TU CAMELOPARDI
PRIMARY
SECONDARY
6
4.8
2.4
0.6
-1.2
-3
-4.7
-4.42
-4.14
-3.86
-3.58
-3.3
log Teff
log L/Lo

# TW DRACONIS

$\alpha$ = 15h33m36s  $\delta$ = 63°57'49"

Ephem: 33888.452 + 2.80687E

Primary Eclipse = Occulting

| | | X | V | B | U | (b-v) | (u-b) |
|---|---|---|---|---|---|---|---|
| Totality: | 21 Apr | 1.027 | 5201 | 2048 | 143 | 1.012 | 2.89 |
| Out: | 16 Apr | 1.214 | 5216 | 4369 | 845 | .192 | 1.784 |

Reduced Color Indices:

$(B-V)_b$ = .193  $(B-V)_1$ = 1.164
$(U-v)_b$ = .267  $(U-V)_1$ = 2.332

$m_b$ = 7.5  $m_{tot}$ = 9.8

Normalized Counts:

$V_b$ = 5216  $V_1$ = 522
$B_b$ = 4367  $B_1$ = 178
$U_b$ = 4079  $U_1$ = 61

New Color Indices: $(B-V)_2$ = .122  $(U-V)_2$ = .166

Spectral Classes: Primary - A3V
Secondary - K2IV

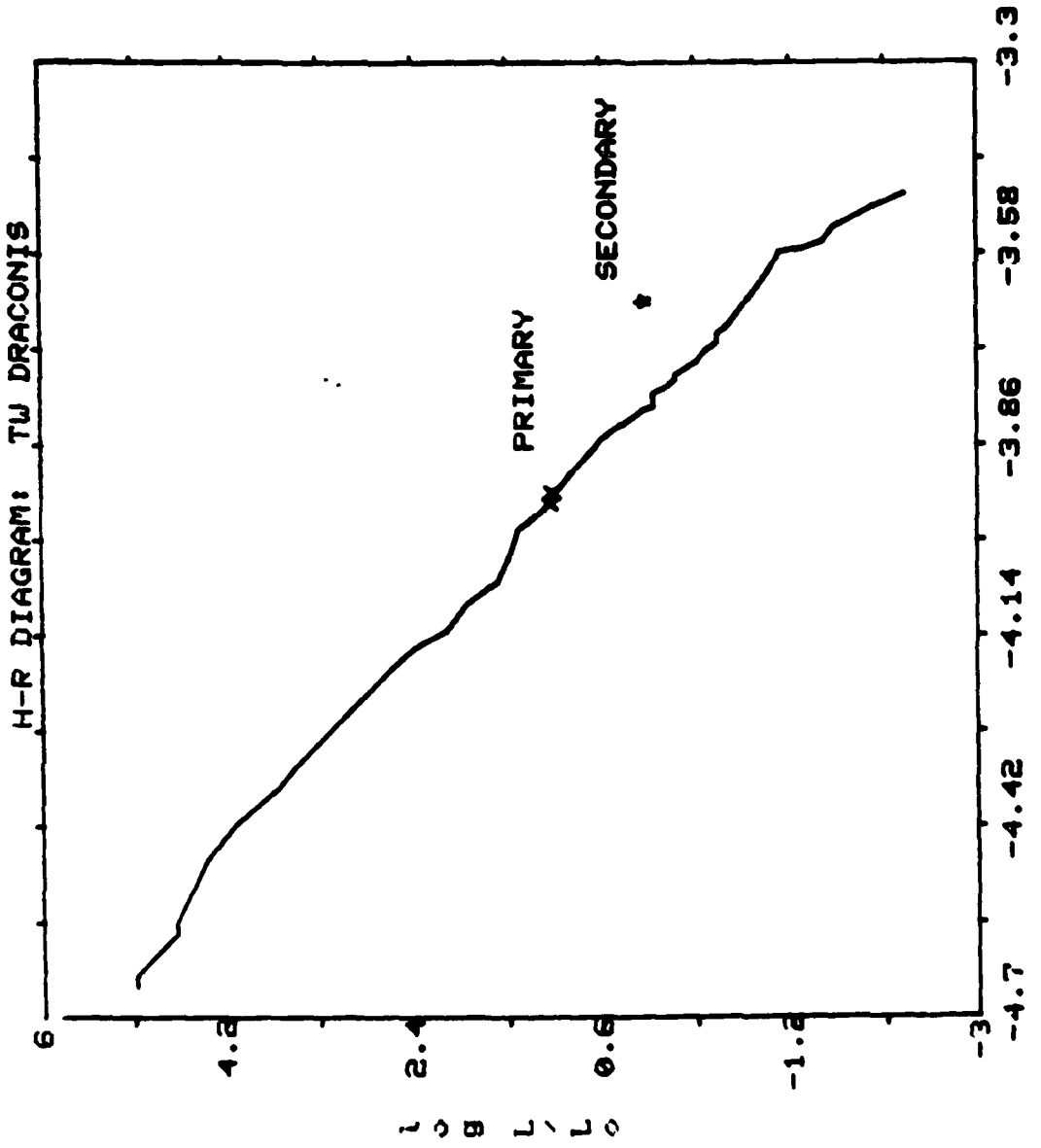
H-R DIAGRAM: TW DRACONIS
SECONDARY
PRIMARY
6
4.8
2.4
0.6
-1.8
-3
-4.7
-4.42
-4.14
-3.86
-3.58
-3.3
log L/Lo
-log Teff

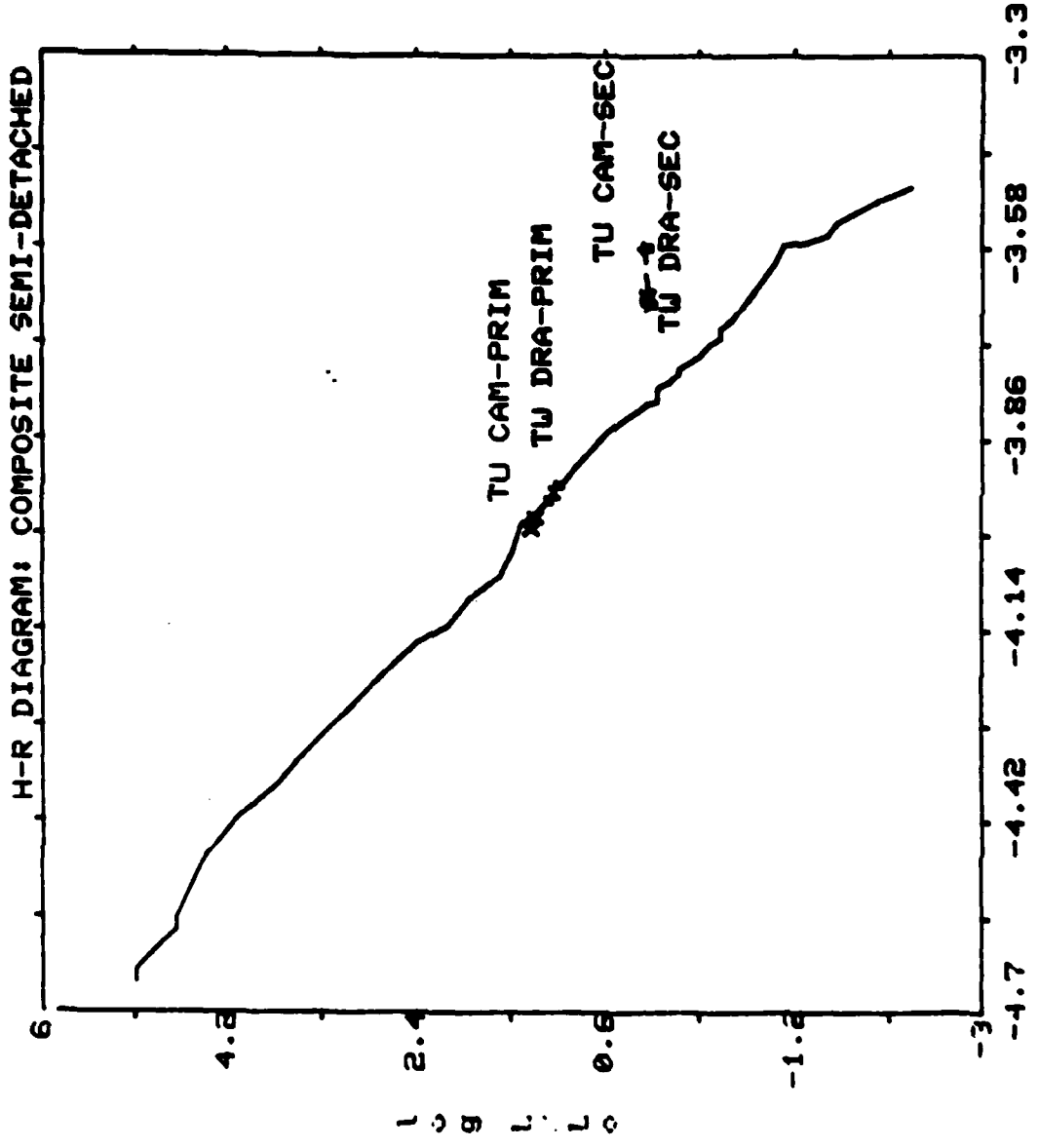
H-R DIAGRAM: COMPOSITE SEMI-DETACHED
TU CAM-PRIM
TU DRA-PRIM
TU CAM-SEC
TU DRA-SEC
6
4.8
2.4
0.6
-1.8
-3
-4.7
-4.42
-4.14
-3.86
-3.58
-3.3
-log Teff

# W URSAE MAJORIS

$\alpha$ = 09h42m34s  $\delta$ = 56°01'49"

Ephem: 2434489.44286 + .3336384E

Primary Eclipse = Occulting

| | | X | V | B | U | (b-v) | (u-b) |
|---|---|---|---|---|---|---|---|
| Totality: | 2 Mar | 1.056 | 4070 | 2450 | 428 | .551 | 1.894 |
| | 15 Mar | 1.111 | 3458 | 2337 | 386 | .425 | 1.955 |
| Out: | 2 Mar | 1.070 | 4244 | 2516 | 484 | .568 | 1.790 |
| | 2 Mar | 1.181 | 4459 | 2918 | 514 | .575 | 1.885 |

Reduced Color Indices:

$(B-V)_b$ = .590  $(B-V)_1$ = .584
$(U-V)_b$ = .698  $(U-V)_1$ = .759

$m_b$ = 8.5  $m_{tot}$ = 9.2

Normalized Counts:

$V_b$ = 4349  $V_1$ = 2282
$B_b$ = 2526  $B_1$ = 1333
$U_b$ = 2287  $U_1$ = 1134

New Color Indices:  $(B-V)_2$ = .597  $(U-V)_2$ = .657

Specral Classes:  Primary - G0V
Secondary - F9V

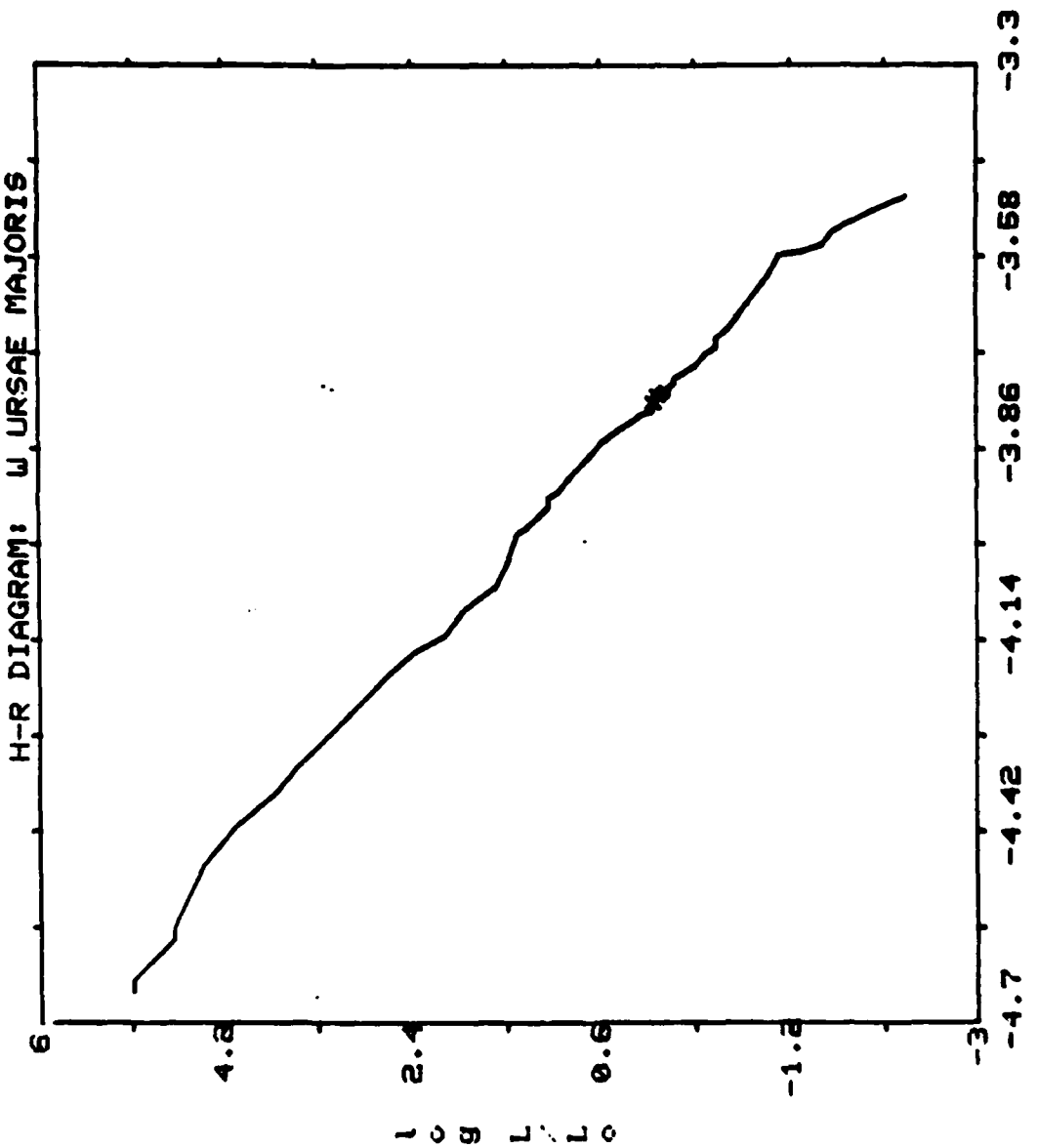
H-R DIAGRAM: W URSAE MAJORIS
6
4.8
2.4
0.6
-1.2
-3
log L/Lo
-4.7
-4.42
-4.14
-3.86
-3.58
-3.3
-log Teff

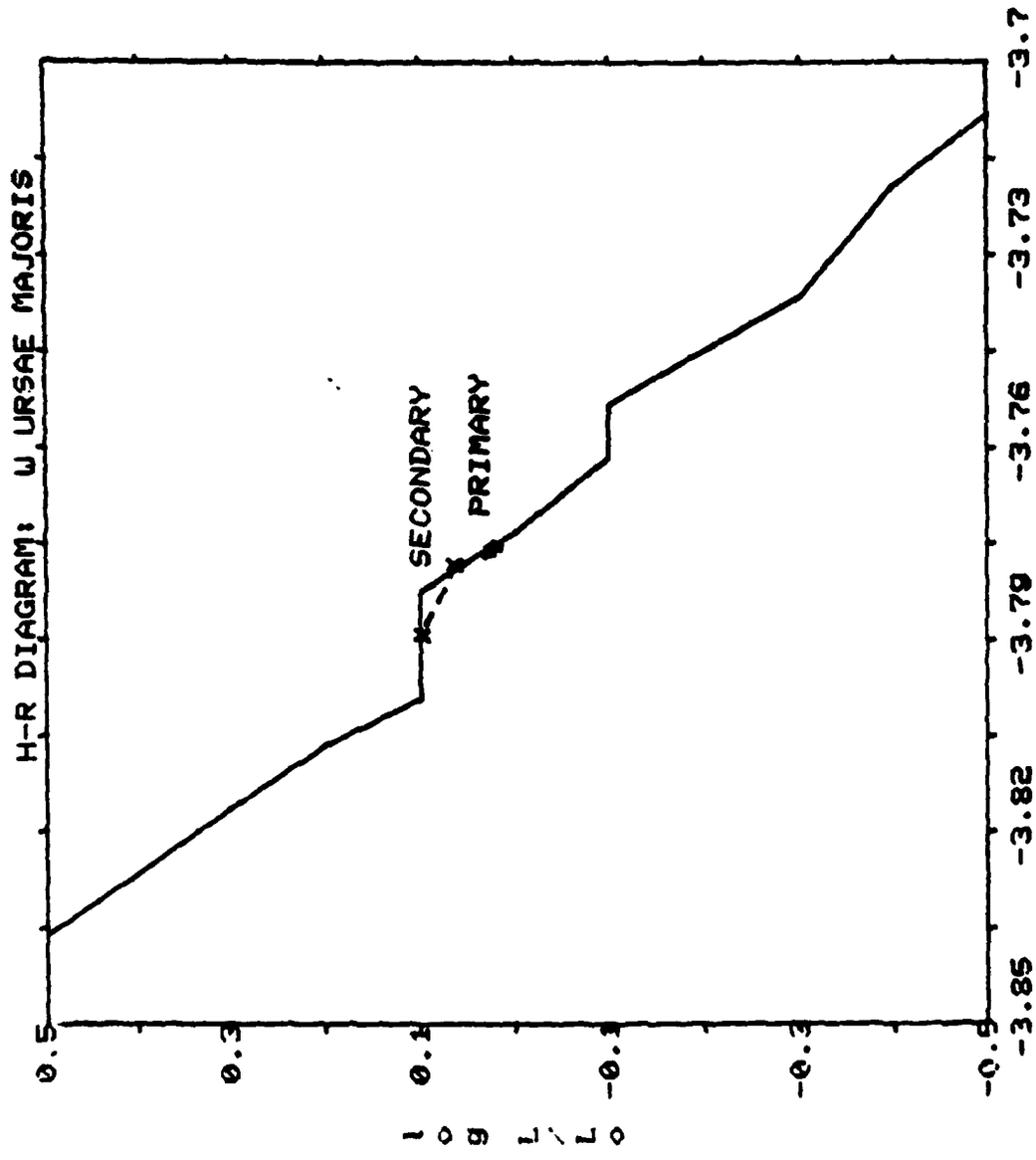
H-R DIAGRAM: U URSAE MAJORIS
SECONDARY
PRIMARY
log L/L⊙
0.5
0.3
0.1
-0.1
-0.3
-0.5
-3.85
-3.82
-3.79
-3.76
-3.73
-3.7
-log Teff

# V566 OPHIUCHI

$\alpha$ = 17h56m02s  $\delta = 4^{\circ}59'16''$

Ephem: 2435245.544 + .40964101E

Primary Eclipse = Annular

| | | X | V | B | U | (b-v) | (u-b) |
|---|---|---|---|---|---|---|---|
| Totality: | 16 Apr | 1.263 | 5526 | 3921 | 816 | .373 | 1.784 |
| Out: | 20 Apr | 1.250 | 4442 | 3066 | 666 | .403 | 1.658 |
| | 21 Apr | 1.219 | 4751 | 2031 | 595 | .488 | 1.768 |

Reduced Color Indices:

$(B-V)_b = .461$  $(B-V)_1 = .449$

$(U-V)_b = .488$  $(U-V)_1 = .523$

$m_b = 7.5$  $m_{tot} = 7.9$

Normalized Counts:

$V_b = 4597$  $V_1 = 3180$

$B_b = 3007$  $B_1 = 2103$

$U_b = 2933$  $U_1 = 1964$

New Color indices: $(B-V)_2 = .490$  $(U-V)_2 = .413$

Spectral Classes: Primary - F6V
Secondary - F5.5V

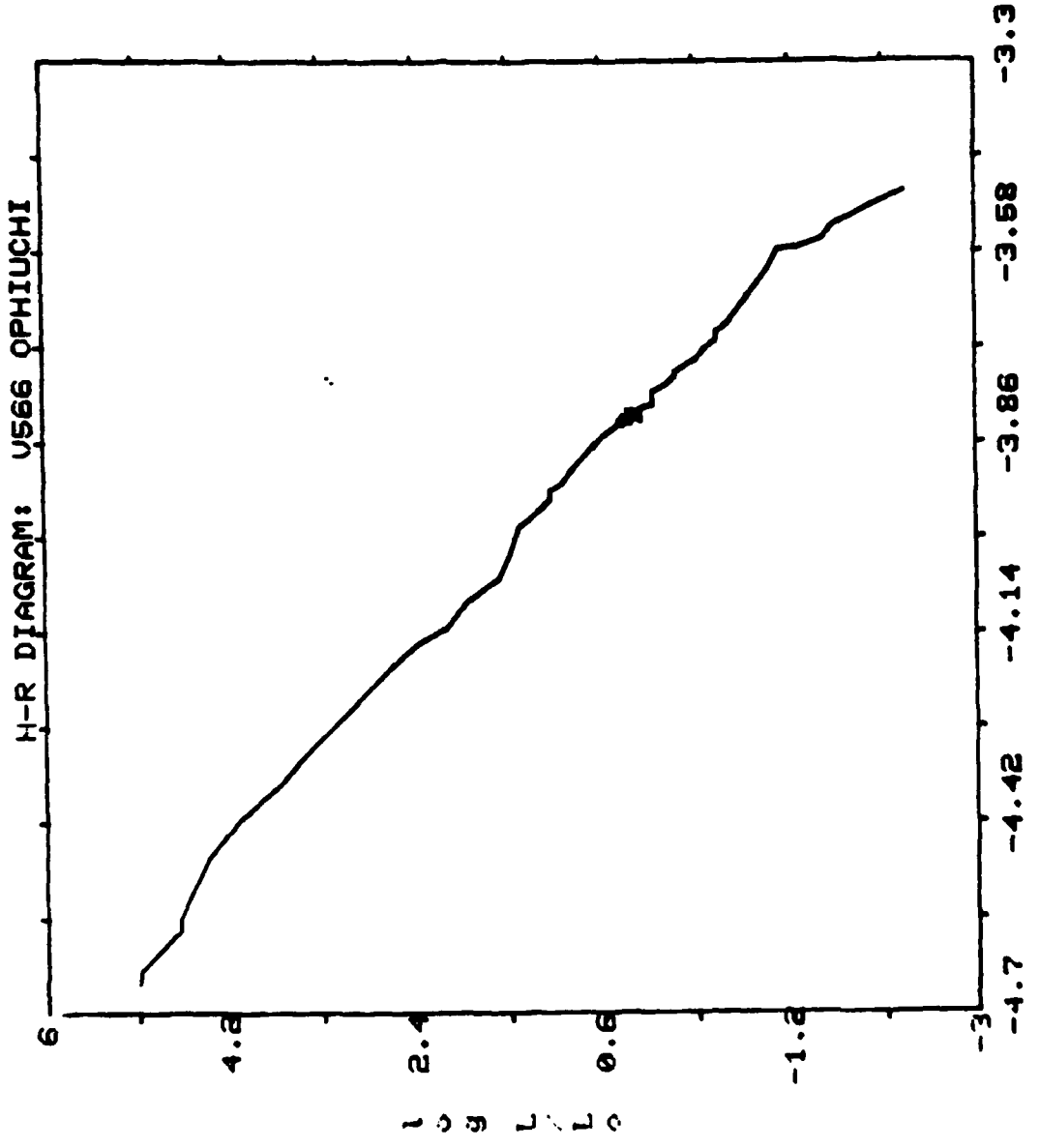
H-R DIAGRAM: V566 OPHIUCHI
6
4.8
2.4
0.6
-1.2
-3
-4.7
-4.42
-4.14
-3.86
-3.58
-3.3
-log Teff

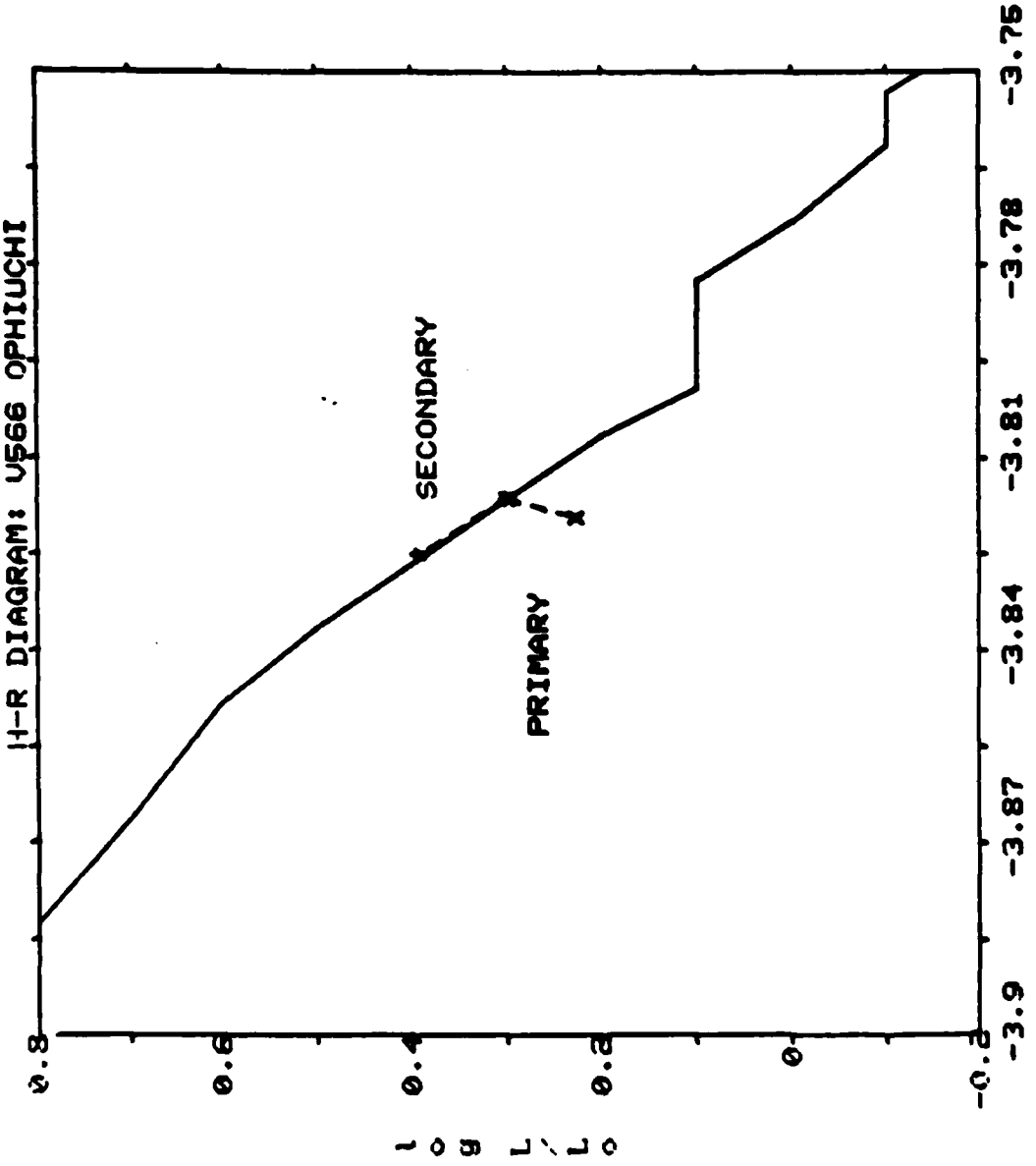
H-R DIAGRAM: U566 OPHIUCHI
SECONDARY
PRIMARY
0.8
0.6
0.4
0.2
0
-0.2
log L/Lo
-3.9
-3.87
-3.84
-3.81
-3.78
-3.75
-log Teff

# AK HERCULIS

$\alpha$ = 17h13m12s  $\delta$ = 16°22'15"

Ephem: 2436757.6601 + .42152502E

Primary Eclipse = Annular

| | | X | V | B | U | (b-v) | (u-b) |
|---|---|---|---|---|---|---|---|
| Totality: | 20 Apr | 1.149 | 2007 | 1283 | 256 | .486 | 1.75 |
| Out: | 16 Apr | 1.417 | 2022 | 1458 | 279 | .413 | 1.795 |

Reduced Color Indices:

$(B-V)_b$ = .459  $(B-V)_1$ = .536
$(U-V)_b$ = .544  $(U-V)_1$ = .607

$m_b$ = 8.5  $m_{tot}$ = 8.9

Normalized Counts:

$V_b$ = 2022  $V_1$ = 1399
$B_b$ = 1325  $B_1$ = 854
$U_b$ = 1225  $U_1$ = 800

New Color Indices: $(B-V)_2$ = .302  $(U-V)_2$ = .416

Spectral Classes: Primary - F8V
Secondary - F1V

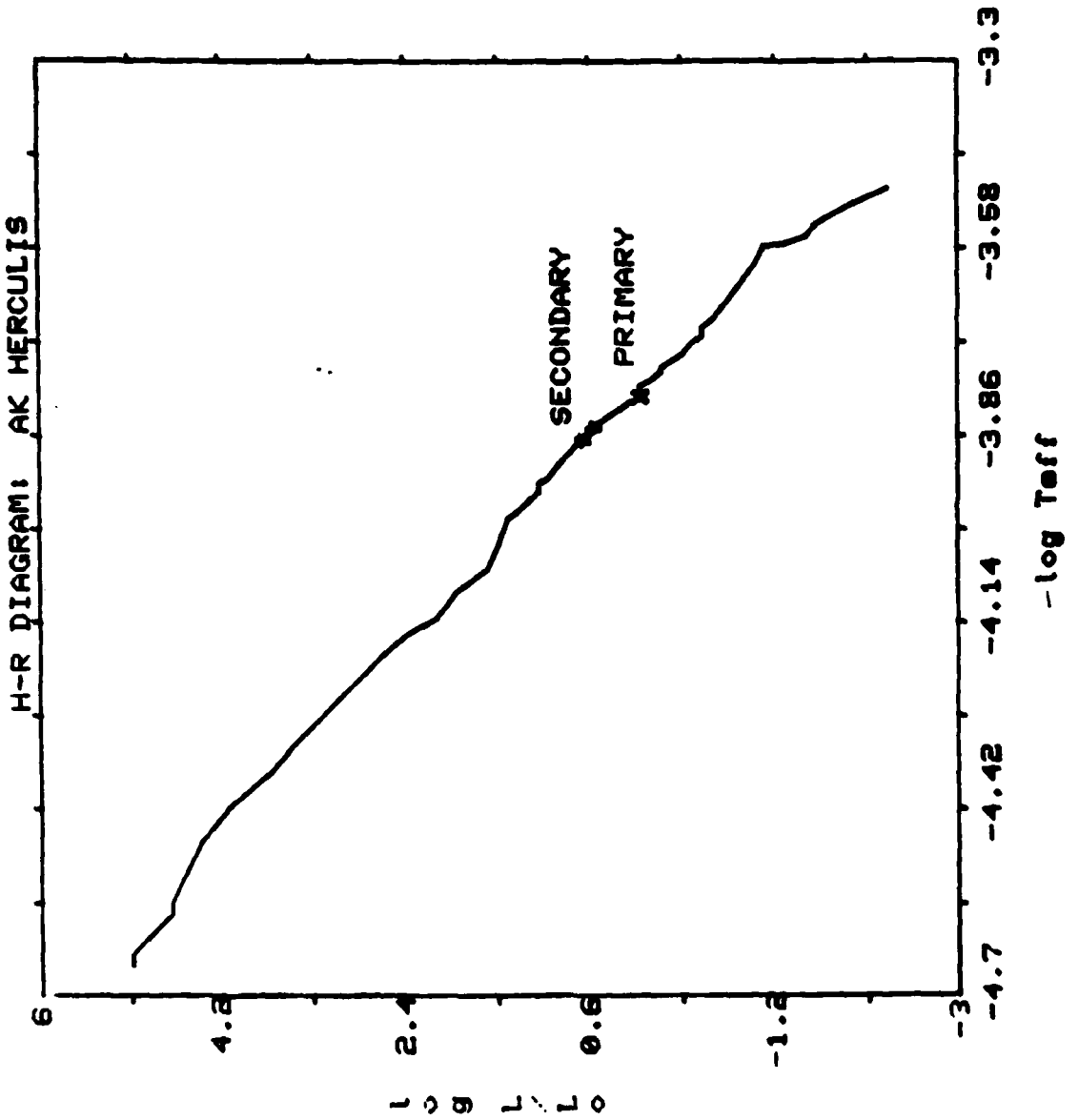
H-R DIAGRAM: AK HERCULIS
SECONDARY
PRIMARY
6
4.8
2.4
0.6
-1.2
-3
log L/Lo
-4.7
-4.42
-4.14
-3.86
-3.58
-3.3
-log Teff

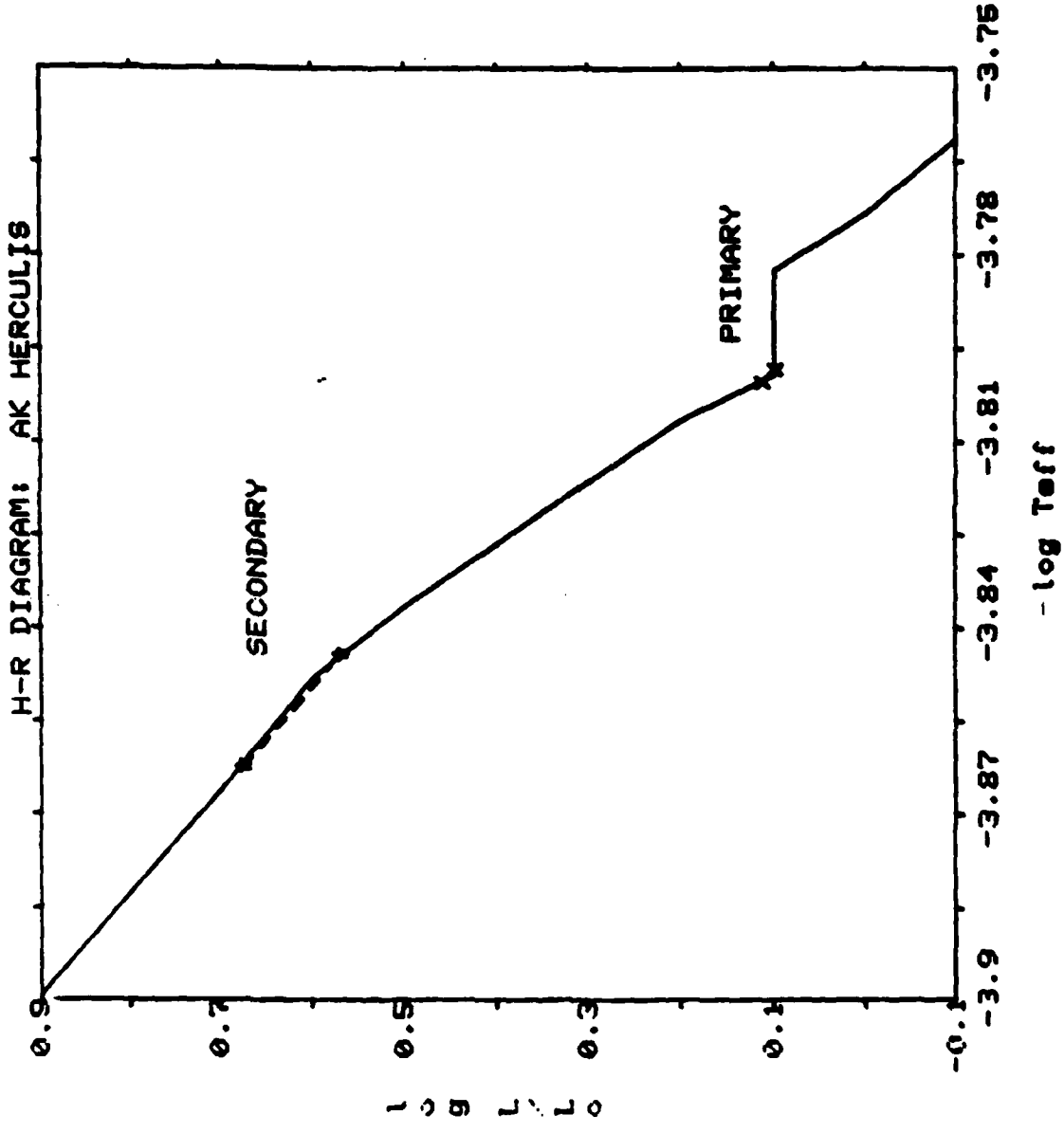
H-R DIAGRAM: AK HERCULIS
SECONDARY
PRIMARY
log L/Lo
- log Teff
0.9
0.7
0.5
0.3
0.1
-0.1
-3.9
-3.87
-3.84
-3.81
-3.78
-3.75

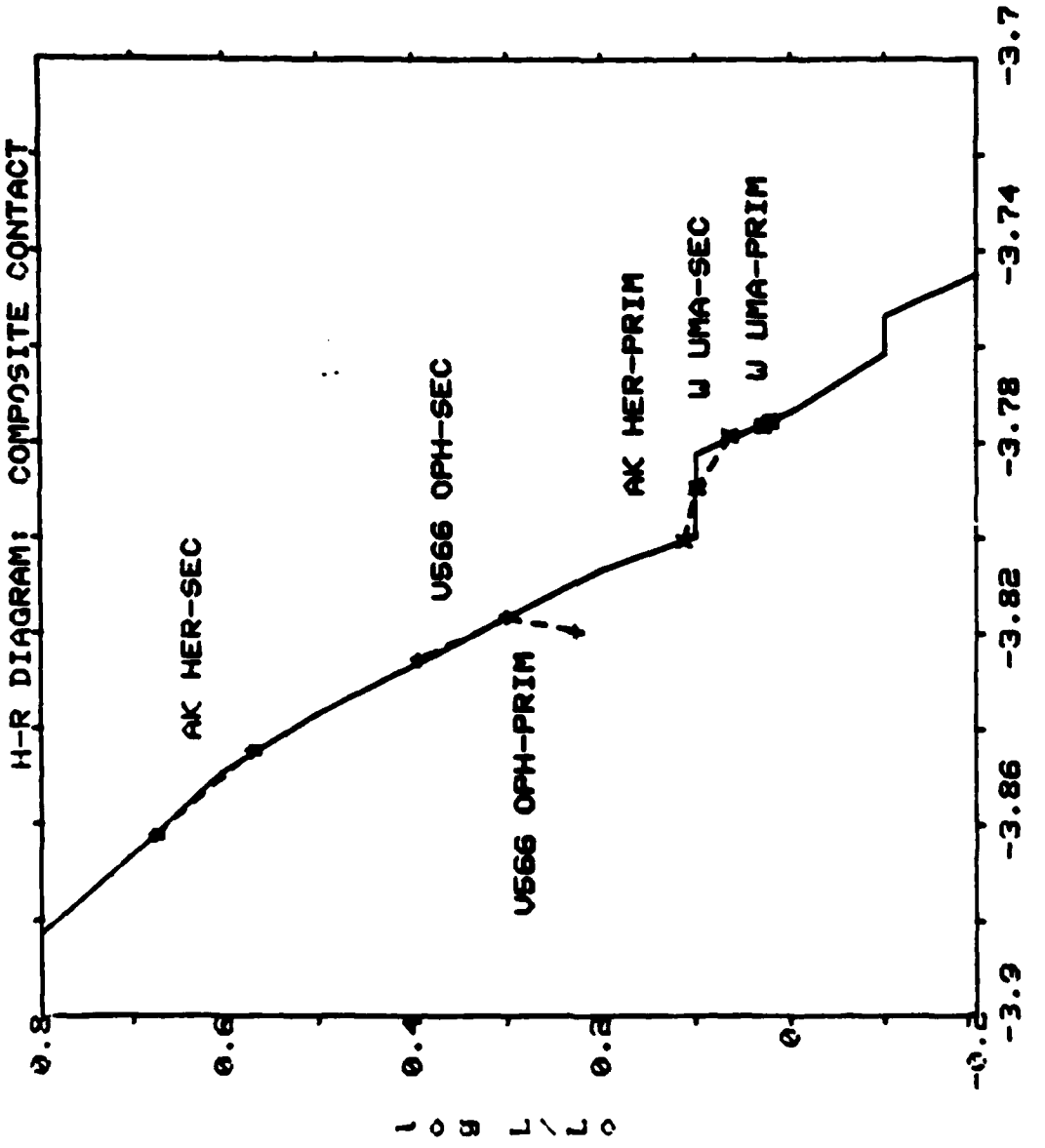
H-R DIAGRAM: COMPOSITE CONTACT
AK HER-SEC
V566 OPH-SEC
V566 OPH-PRIM
AK HER-PRIM
U UMA-SEC
U UMA-PRIM
0.8
0.6
0.4
0.2
0
-0.2
-3.9
-3.86
-3.82
-3.78
-3.74
-3.7
log L/Lo
-log Teff

# AG VIRGINIS

$\alpha$ = 12h00m11s  $\delta$ = 13°06'10"

Ephem: 2434086.4176 + .64264907E

Primary Eclipse = Annular

| | | X | V | B | U | (b-v) | (u-b) |
|---|---|---|---|---|---|---|---|
| Totality: | 16 Apr | 1.094 | 1502 | 1320 | 261 | .14 | 1.76 |
| Out: | 15 Mar | 1.124 | 2227 | 1871 | 329 | .189 | 1.89 |
| | 23 Mar | 1.224 | 2626 | 2423 | 525 | .087 | 1.66 |

Reduced Color Indices:

$(B-V)_b$ = .132  $(B-V)_1$ = .068
$(U-V)_b$ = .193  $(U-V)_1$ = .127

$m_b$ = 9.0  $m_{tot}$ = 9.4

Normalized Counts:

$V_b$ = 2427  $V_1$ = 1680
$B_b$ = 2149  $B_1$ = 1578
$U_b$ = 2032  $U_1$ = 1495

New Color Indices: $(B-V)_2$ = .295  $(U-V)_2$ = .363

Spectral Classes: Primary - A2V
Secondary - A9V

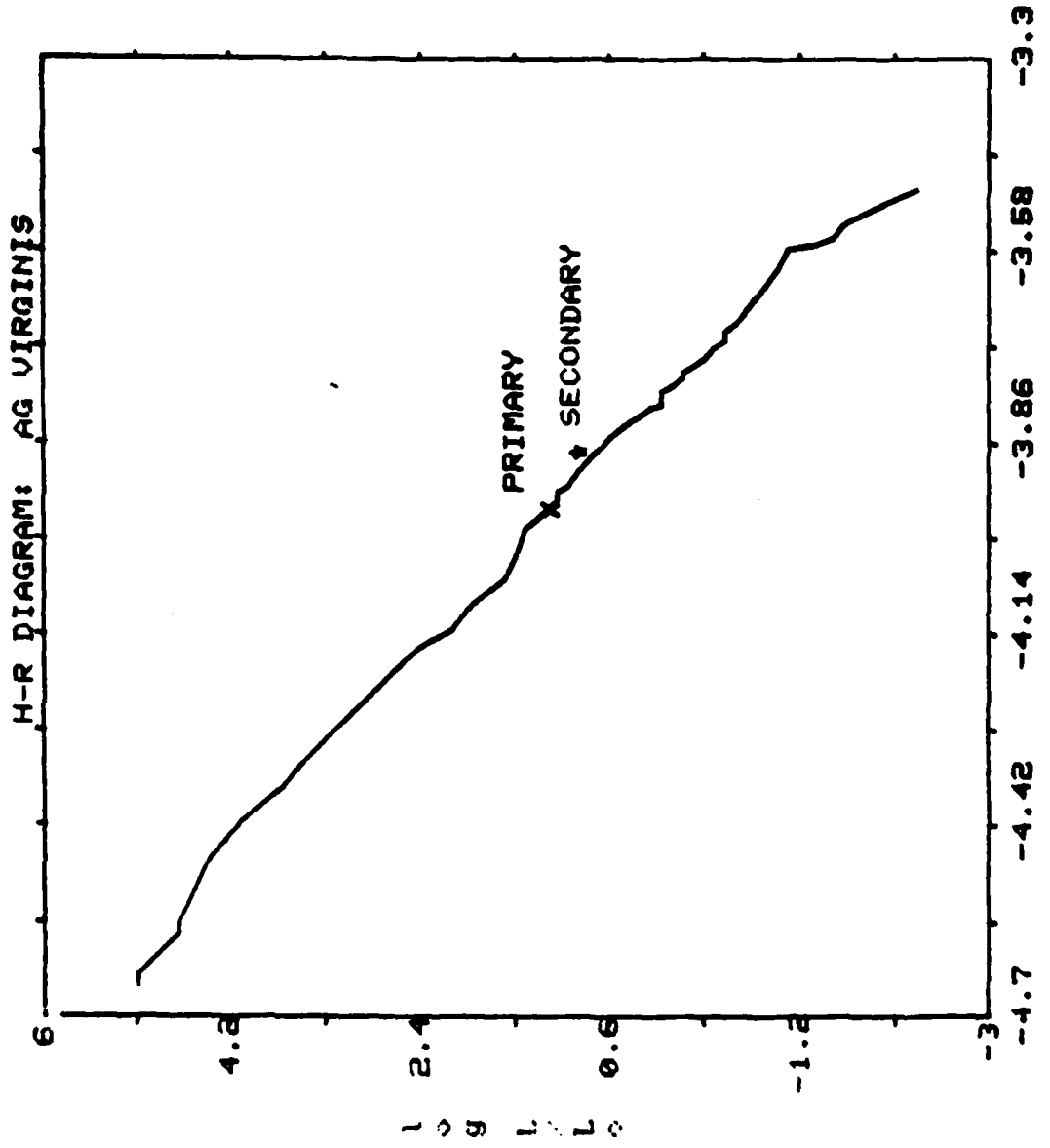
H-R DIAGRAM: AG VIRGINIS
PRIMARY
SECONDARY
6
4.8
2.4
0.6
-1.2
-3
-4.7
-4.42
-4.14
-3.86
-3.58
-3.3
-log Teff

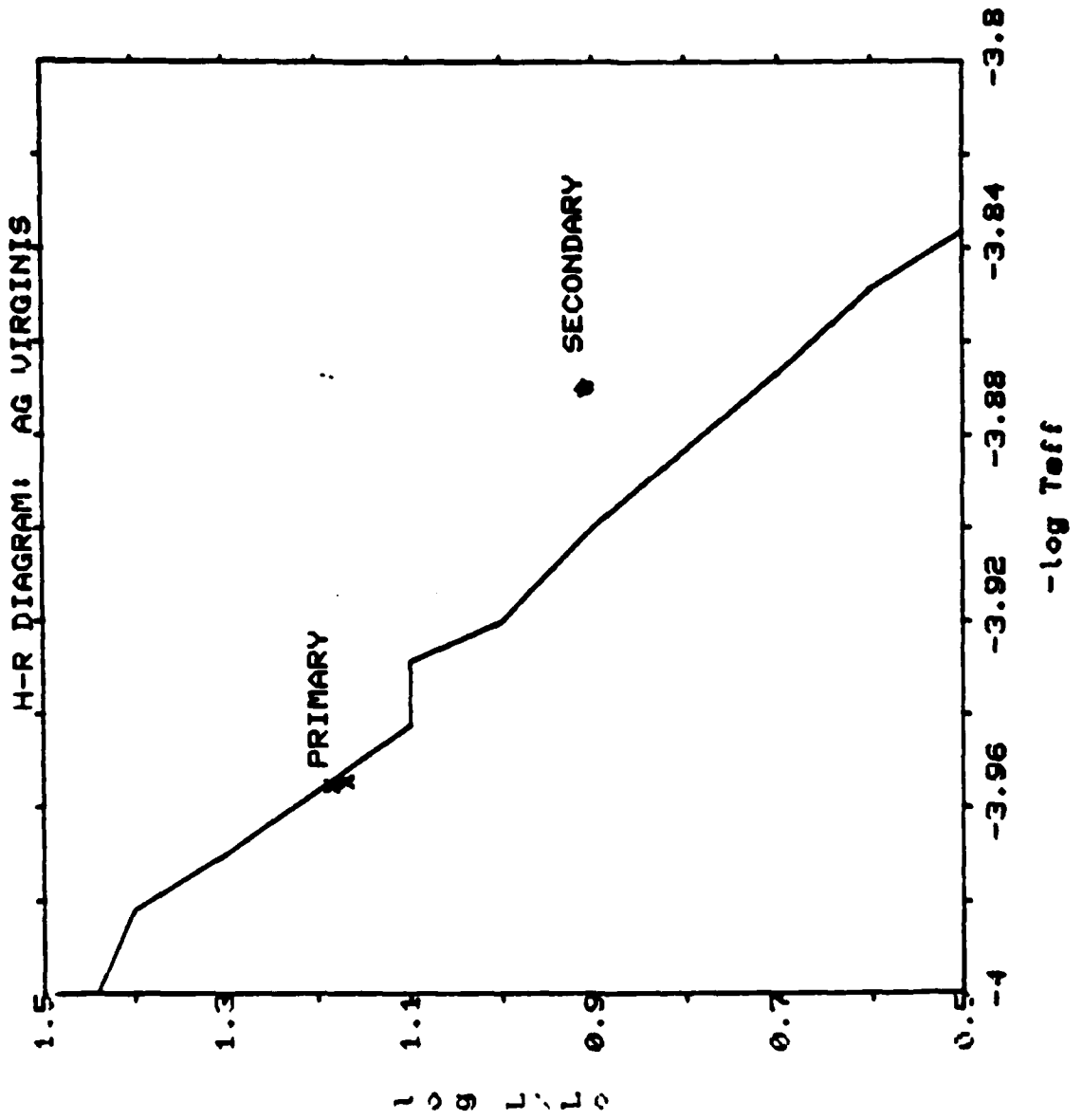
H-R DIAGRAM: AG VIRGINIS
PRIMARY
SECONDARY
1.5
1.3
1.1
0.9
0.7
0.5
-3.8
-3.84
-3.88
-3.92
-3.96
-4
-log Teff

## α CORONA BOREALIS

α = 15h33m58s  δ = 26°46'20"

Ephem: 2423163.770 + 17.359907E

Primary Eclipse = Annular

---

| | | X | V | B | U | (b-v) | (u-b) |
|---|---|---|---|---|---|---|---|
| Totality: | 20 Apr | 1.076 | 759610 | 738445 | 165824 | .031 | 1.622 |

Reduced Color Indices: $(B-V)_1 = -.108$
$(U-V)_1 = -.169$

Spectral Class: Primary - B9V

# AM LEONIS

$\alpha$ = 11h01m18s  $\delta = 9^{\circ}59'21''$

Ephem: 2435593.7168 + .36579912E

Primary Eclipse = Occulting

---

| | | X | V | B | U | (b-v) | (u-b) |
|---|---|---|---|---|---|---|---|
| Totality: | 12 Apr | 1.201 | 864 | 553 | 81 | .484 | 1.983 |

Reduced Color Indices: $(B-V)_1 = .485$
$(U-V)_1 = .633$

Spectral Class: Secondary - F7V

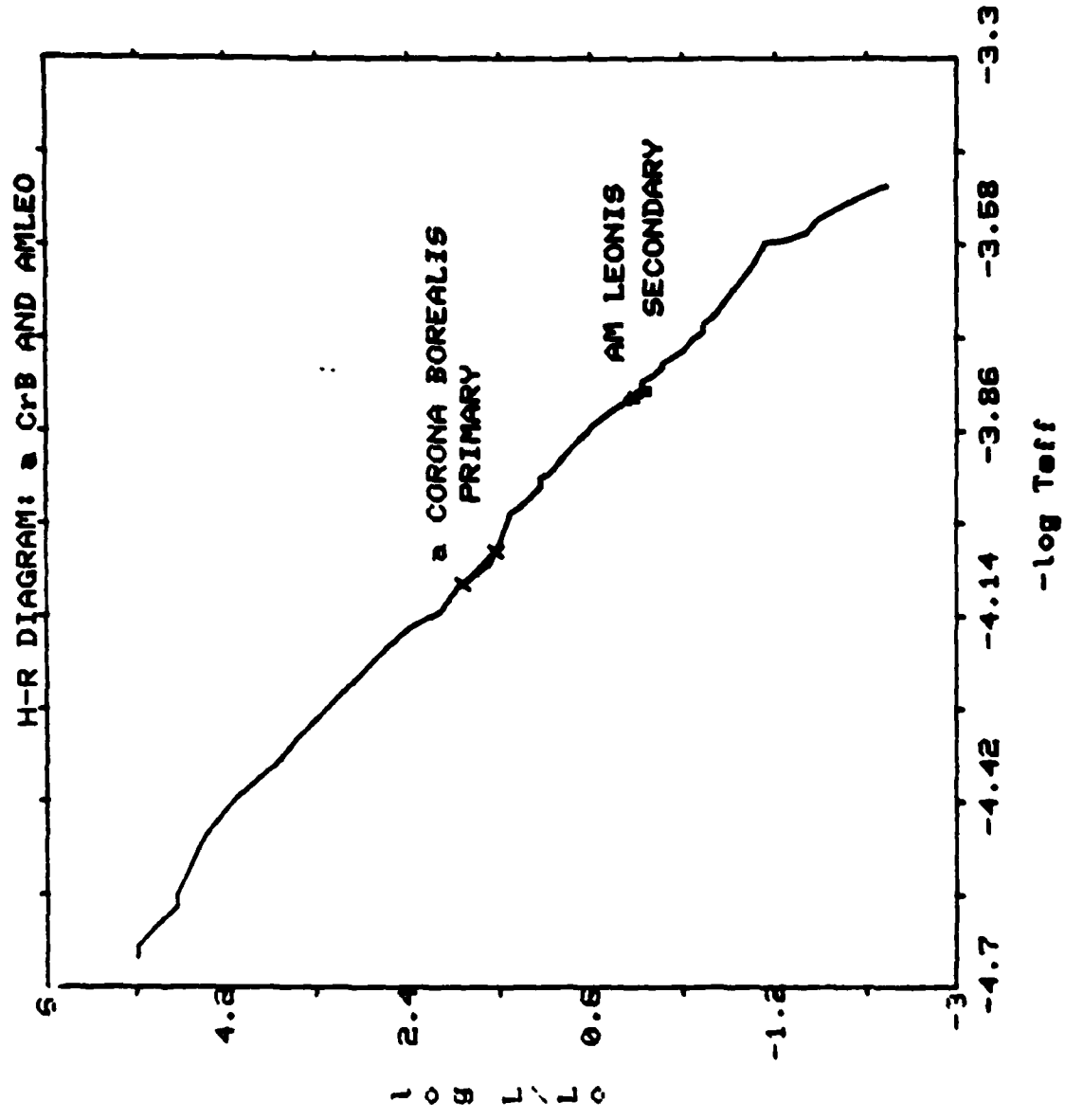
H-R DIAGRAM: α CrB AND AMLEO
α CORONA BOREALIS
PRIMARY
AM LEONIS
SECONDARY
4.8
2.4
0.6
-1.8
-3
-4.7
-4.42
-4.14
-3.86
-3.58
-3.3
log L/L⊙
-log Teff

## TZ BOOTES

$\alpha$ = 15h07m32s $\delta = 40^{\circ}02'01''$

Ephem: 2432701.428 + .29716E

| | | X | V | B | U | (b-v) | (u-b) |
|---|---|---|---|---|---|---|---|
| Out: | 23 Mar | 1.003 | 2846 | 564 | 96 | 1.76 | 1.92 |

Reduced Color Indices: $(B-V)_b = 2.067$
$(U-V)_b = 2.325$

## RS CANES VENATICI

$\alpha$ = 13n09m50s $\delta = 36^{\circ}01'29''$

Ephem: 2433016.819 + 4.79781E

| | | X | V | B | U | (b-v) | (u-b) |
|---|---|---|---|---|---|---|---|
| Out: | 12 Apr | 1.012 | 3599 | 2071 | 387 | .588 | 1.821 |

Reduced Color Indices: $(B-V)_b = .632$
$(u-V)_b = .680$

The H-R diagrams of TU Camelopardi and TW Draconis strongly suggest that they are semi-detached systems. Both primaries are relatively large main sequence stars (spectral classes A1V and A3V), and both secondaries are above the main sequence, as we would expect for a contact secondary with a diffuse atmosphere. Both periods are about 2.8 days, also what we would expect for a semi-detached system.

Similarly, the diagrams of W Ursae Majoris, V566 Ophiuchi, and AK Herculis suggest that these are all contact systems. The large scale diagram shows that both components in any system are grouped around the main sequence. The small scale diagram shows that the secondary is the brighter in all three cases, although both components have about the same temperature. All of the components, whether primary or secondary, fall within a very limited spectral class range, from F1V to G0V, with most being late (F6→F9). This uniformity among the components is in agreement with theoretical predictions stemming from tidal forces as discussed in the first section. The periods of these systems, 0.33 to 0.46 days, also suggest contact binary status.

The system AG Virginis presents a unique problem. Its period, .62 days, is within the expected range of periods for contact systems. However, the spectral classes of its components, A2V and A9V, are not what we would expect in a contact system, and its primary is brighter, also in contradiction of our expectations. The components are also of the wrong spectral classes to be a semi-detached system, as their positions on the H-R diagram, at a quick glance, may suggest.

Thus we are left with the possibility of a detached system. There is nothing in the photometric elements of the results which would disallow this; we expect the primary to be hotter and more luminous in a detached pair, and such a system has no real restrictions on component spectral class. Unfortunately, the period is very short for a detached pair. One method for decreasing the period while maintaining separation is to increase orbital speed. If, however, the stars did revolve about each other at high speeds, their atmospheres would become distended, as though the stars were leaving wakes. This would cause both components to move somewhat above the main sequence, which does not occur in the primary.

A more intriguing possibility, although one requiring further study far beyond the time frame of this project, is that this system is in a state of change. Suppose the system has recently undergone a case B mass transfer. The primary has just settled back to the main sequence (a rapid process), while the secondary is starting to move off, due to its newly acquired atmosphere. Recalling Figure 1-5, the secondary will continue to move off into the giant or sub-giant region, and the system would become semi-detached. Further study may bear out the validity of this hypothesis, but even though greatly accelerated due to the artificial prodding of mass transfer, the transit to the giant region will be measured in millennia.

One may similarly hypothesize that the secondary is in transit, not away from, but to the main sequence. This, however, can explain fewer observed features of the system. Most importantly,

a pre-main sequence star at the secondary's position would not have an overly diffuse atmosphere, so that the problem of the short period still remains. Also, the star could take up to $10^7$ years to settle on the main sequence, so that we would not have the opportunity to verify if this is indeed occurring for quite a while. The hypothesis of accelerated secondary transit away from the main sequence following case B mass transfer, leading to a semi-detached configuration, while not without fault, can best explain both the physical and photometric features of the system, and it is also the easiest to observationally investigate.

The H-R diagram for α Corona Borealis and AM Leonis shows just one star from each system since these were observed only at totality. We can predict, however, based on their periods and the location of one of their components, to what kind of system each belongs. With a B9V primary and a long period, α Corona Borealis is either a detached or semi-detached system. AM Leonis, on the other hand, with an F7V secondary and a short period, is in all probability a contact system. No information useful on an H-R diagram could be determined for TZ Bootes and RS Canes Venatici, since these systems were observed only out of eclipse.

# V - CONCLUSIONS

The individual temperatures and luminosities of both components were determined for six binary systems, as summarized below:

| SYSTEM | PRIMARY | SECONDARY | SYSTEM TYPE |
|---|---|---|---|
| TU Cam | A1V | K4IV | Semi-Detached |
| TW Dra | A3V | K2IV | Semi-Detached |
| AK Her | F8V | F1V | Contact |
| V566 Oph | F6V | F5.5V | Contact |
| W UMa | G0V | F9V | Contact |
| AG Vir | A2V | A9V | - |

AG Virginis does not fit neatly into a particular system type. Its photometric elements suggest a detached pair, but its period seems too short for such a configuration. It is hypothesized that the secondary is in transit from the main sequence following case B mass transfer. and thus that the system is in the process of becoming semi-detached. Additional study is needed on a long term time scale in order to substantiate this hypothesis.

Solutions for the occulting star were obtained for two additional systems:

| SYSTEM | PRIMARY | SECONDARY |
|---|---|---|
| $\alpha$ CrB | B9V | --- |
| AM Leo | --- | F7V |

The systems TZ Bootes and RS Canes Venatici were observed only out of eclipse, so that no definitive solution for either of their components could be reached. Complete solutions for these last four systems may be obtained, however, with an observation of the proper event.

The reduction method of Harris, as programmed onto the Naval

Academy's computing facilities, proved itself to be quite effective in transforming raw observational data. The shortness of the uncertainty bars on the Hertzsprung-Russell diagrams attests to the precision of the method, and the ease with which solutions were reached, after the computer programs had been written, cannot be overstated. But more importantly, besides proving to be precise and fast, the reduction seems accurate, in that it leads to final results consistent with theoretical expectations. These factors make this method highly recommendable to any photometric program.

FOOTNOTES

[1] George O. Abell, Exploration of the Universe, (Philadelphia: Saunders Publishing, 1982), p. 455.

[2] Eva Novotny, Introduction to Stellar Atmospheres, (New York: Oxford University Press, 1973), p. 280.

[3] ibid, p. 282.

[4] ibid, p. 285.

[5] I. Iben, Jr., "Stellar Evolution: The Approach to the Main Sequence", Astrophysical Journal, V141 (1 April 1965): 1010.

[6] Novotny, p. 285.

[7] Robert F. Stein, "Stellar Evolution: A Survey with Analytic Models", in Stellar Evolution, Ed. R.F. Stein and A.G.W. Cameron, (New York: Plenum Press, 1966), p. 44.

[8] ibid., p. 27.

[9] Novotny, p. 324.

[10] Stein, p. 40.

[11] Novotny, p. 327.

[12] Khushiro Hayashi, "Advanced Stages of Stellar Evolution", in Stellar Evolution, Ed. R.F. Stein and A.G.W. Cameron, (New York: Plenum Press, 1966), p. 254.

[13] Novotny, p. 321.

[14] Wulff D. Heintz, Double Stars, (Dordreicht: D. Reidel Publishing Co., 1978), p. 128.

[15] Zdenek Kopal, Close Binary Systems, (New York: John Wiley and Sons, Inc., 1959), p. 185.

[16] ibid., p. 170.

[17] Heintz, pp. 94ff.

[18] Kopal, p. 133.

[19] Heintz, p. 123.

[20] Kopal, section VII-5.

[21] Heintz, p. 119.

[22] Heintz, p. 121.

[23] Kopal, pp. 467ff.

[24] Heintz, p. 130.

[25] H.L. Johnson and W.W. Morgan, "Fundamental Stellar Photometry for Standards of Spectral Type on the Revised System of the Yerkes Spectral Atlas", Astrophysical Journal, V117 (1 May 1953): 321.

[26] C.W. Allen, Astrophysical Quantities, (London: The Athlone Press, 1973), pp. 200ff.

[27] W.E. Harris, M.P. Fitzgerald, and B.C. Reed, "Photoelectric Photometry: An Approach to Data Reduction", Publications of the Astronomical Society of the Pacific, V. 93, (August 1981): 507-517.

[28] Richard L. Walker, private communication: 4 December 1981, 16 June 1982.

[29] Johnson and Morgan, pp. 323-327.

[30] R.H. Koch, S. Sobieski, and F.B. Wood, Finding List for Observers of Eclipsing Variables, (Philadelphia: University of Pennsylvania Press, 1963).

[31] J.B. Rafert, "Periodic Ephemerides for Forty-nine Eclipsing Binary Star Systems", Publications of the Astronomical Society of the Pacific, V94 (June 1982): 485-496.

[32] V.I. Kurkarkin, et. al., Publications of the Sternberg State Astronomical Institute of Moscow State University, (Moscow: Moscow University Press, 1970).

[33] Rex H. Shudde, private communication.

[34] The Smithsonian Astrophysical Observatory Star Atlas, (Cambridge: Harvard University Press, 1968).

[35] Harris, et. al., p. 509.

[36] Kurkarkin, et. al.

[37] Novotny, pp. 10ff.

[38] Walker, private communication.

[39] D.D. Clayton, Principles of Stellar Evolution and Nucleosynthesis, (New York: McGraw-Hill, 1968), pp. 380ff.

[40] ibid., pp. 380ff.

# BIBLIOGRAPHY


Abell, George O. Exploration of the Universe. Philadelphia: Saunders Publishing Co., 1982.

Allen, C.W. Astrophysical Quantities. London: The Plenum Press, 1972.

Clayton, D.D. Principles of Stellar Evolution and Nucleosynthesis. New York: McGraw-Hill, 1965.

Harris, W.E., Fitzgerald, M.P., and Reed, B.C. "Photoelectric Photometry: An Approach to Data Reduction." Publications of the Astronomical Society of the Pacific. V93 (August 1981): 507-518.

Hayashi, Khushiro. "Advanced Stages of Stellar Evolution." In Stellar Evolution. Ed. R.F. Stein and A.G.W. Cameron. New York: The Plenum Press, 1966.

Heintz, Wulff D. Double Stars. Dordreicht: D. Reidel Publishing Co., 1978.

Iben, I. Jr. "Stellar Evolution: The Approach to the Main Sequence." Astrophysical Journal. V141 (1 April 1965): 1010.

Johnson, H.L. and Morgan, W.W. "Fundamental Stellar Photometry for Standards of Spectral Type on the Revised System of the Yerkes Spectral Atlas." Astrophysical Journal. V117 (1 May 1953): 313-352.

Koch, Robert H., Sobieski, Stanley, and Wood, Frank B. Finding List for Observers of Eclipsing Variables. Philadelphia: University of Pennsylvania Press, 1963.

Kopal, Zdenek. Close Binary Systems. New York: John Wiley and Sons, Inc., 1959.

Kurkarkin, V.I., et. al. Publications of the Sternberg State Astronomical Institute of Moscow State University. Moscow: Moscow State University Press, 1970.

Novotny, Eva. Introduction to Stellar Atmospheres. New York: Oxford University Press, 1973.

Rafert, J.B. "Periodic Ephemerides for Forty-nine Eclipsing Binary Star Systems." Publications of the Astronomical Society of the Pacific. V94 (June 1982): 485-496.

Shudde, Rex H. Private communication.

Stein, Robert F. "Stellar Evolution: A Survey with Analytic Models." In Stellar Evolution. Ed. R.F. Stein and A.G.W. Cameron. New York: Plenum Press, 1966.

Walker, Richard L. Private communication.

# APPENDIX I

## NUCLEAR FUEL CYCLES

The three most important fusion cycles to stellar energy generation are the proton-proton chain, the carbon-nitrogen-oxygen cycle, and the triple-alpha chain. Each will be analyzed, concentrating on energy generated, fractional mass loss per cycle, and energy loss through neutrinos.

I Proton-Proton Chain ($T < 15 \times 10^6$ K)

| | |
|---|---|
| $\alpha)\ 2^{\times}$: $H^1 + H^1 \rightarrow D^2 + e^+ + \nu$ | $E_e + E_\nu = 1.4421$ MeV |
| $\beta)\ 2^{\times}$: $D^2 + H^1 \rightarrow He^3 + \gamma$ | $E_\gamma = 5.4935$ MeV |
| $\gamma)\ He^3 + He^3 \rightarrow He^4 + H^1 + H^1$ | $E = 12.8599$ MeV |
| NET: $4H^1 \rightarrow He^4 + E$ | $E = 26.7312$ MeV |

This net energy release is only 0.7119% of the original mass of the four hydrogens. From this, we can assume that the mass during the main sequence is constant. We can get a rough maximum for the neutrino loss by allowing the positron to rapidly annihilate with an electron, releasing two .511MeV $\gamma$'s, leaving .4201MeV to the neutrino. The average neutrino loss, however, is only about .26MeV,[39] or about 1.945% of the energy produced.

II Carbon-Nitrogen-Oxygen Cycle $(15\times10^6<T<10^8)$

α) $C^{12} + H^1 \rightarrow N^{13} + \gamma$ $E_\gamma = 1.9436MeV$

β) $N^{13} \rightarrow C^{13} + e^+ + \nu$ $E_e + E_\nu = 2.2205MeV$

γ) $C^{13} + H^1 \rightarrow N^{14} + \gamma$ $E_\gamma = 7.5499MeV$

δ) $N^{14} + H^1 \rightarrow O^{15} + \gamma$ $E_\gamma = 7.2922MeV$

ε) $O^{15} \rightarrow N^{15} + e^+ + \nu$ $E_e + E_\nu = 2.7606MeV$

ζ) $N^{15} + H^1 \rightarrow C^{12} + He^4$ $E = 4.9646MeV$

NET: $4H^1 \rightarrow He^4 + E$ $E_t = 26.7312MeV$

The $C^{12}$ acts as a catalyst allowing reaction (α) to go. Again the energy released is only .7119% of the initial mass, giving constant mass during this fusion process. Rough maxima for the neutrino loss are 1.1985MeV for reaction (β) and 1.7386MeV for reaction (ε). More sophisticated treatment gives average neutrino loss as .7105MeV and 1.0006MeV respectively.[40] The total energy loss to neutrinos is therefore 1.7111MeV, or 6.4011% of the total energy. This loss is clearly no longer negligible, and will become an important factor in later evolution, as discussed in section I.

III Triple Alpha Chain $(T>10^8K)$

α) $He^4 + He^4 \rightarrow Be^8 + \gamma$ $E_\gamma = -.094641MeV$

β) $He^4 + Be^8 \rightarrow C^{12} + \gamma$ $E_\gamma = 7.3683MeV$

NET: $3He^4 \rightarrow C^{12} + E$ $E_t = 7.2736MeV$

Since $Be^8$ has an extremely short half-life, $2\times10^{-16}s$, there must be a very high density of $He^4$ for reaction (β) to go. A helium nucleus whose kinetic energy is solely derived from the temperature

can travel only about 1.289Å in one $Be^8$ half-life. The energy released amounts to only .06503% of the mass of the three helium. Additional reactions further convert some of the carbon into oxygen to form the carbon-oxygen core:

$$\gamma)\ He^4 + C^{12} \rightarrow O^{16} + \gamma \qquad E_\gamma = 7.1605MeV$$

$$\text{NET: } 4He^4 \rightarrow O^{16} + E \qquad E_t = 14.9311MeV$$

The net energy released including this final reaction is .09677% of the mass of the four helium.

If there is enough energy, helium will keep fusing with heavier and heavier nulcei ($O^{16}$, $Ne^{20}$, etc.) until $Fe^{56}$ is reached. This has the lowest binding energy per nucleon (most negative) of any nucleus, and thus is an ultimately stable configuration, the end of the stellar line.

# APPENDIX II

## COMPUTER PROGRAMS

This appendix presents the substantial computer programs written by the author in the course of this project. The programs are listed in the order in which they would be used in solving an unknown system.

1. EPH...: Generates a schedule of observable events

2. YLEYN: Takes standard star observational data and calculates $Z_{\mu\sigma}$ and $S_{\sigma}$ to be used in Harris' reduction method.

3. TENSOP: Operates on $Z_{\mu\sigma}$ and $S_{\sigma}$ to give $G_{\mu}$, the reduction coefficient tensor.

```
EPHEM     27 Apr 83  23:16

100 'This program provides a schedule of ephemerices in eastern standard
110 'time for a binary system, given some initial ephemeris and period.
120
130 PRINT "INPUT STAR, DATE-TIME GROUP (MO,D,HR,M,S), AND PERIOD"
140 INPUT S$, M$, D, H, M, S, P
150 J=D+H/24+M/1440+S/86400
160 PRINT
170 PRINT
180 PRINT TAB(22); "EST EPHEMERIDES FOR ";S$
190 PRINT
200 PRINT TAB(5); "OUT OF ECLIPSE"; TAB(43); "TOTALITY"
210 PRINT
220
240 N=1
250 FOR J=J TO 200 STEP P/4
260 A=INT(J)
270 B=J-A
300 C=0
310 READ M1$,D1
313 DATA DEC, 31, JAN, 31, FEB, 28
316 DATA MAR, 31, APR, 30, MAY, 31, BORT, 100
320 C=C+D1
330 IF C=>A THEN  343
340 GOTO 310
343 IF M1$="BORT" THEN 679
345
348 N=N+1
350 D=A-C+D1
360 H=INT(B*24)
370 G1=B*24-H
380 M=INT(G1*60)
390 G2=G1*60-M
400 S=INT(G2*60)
410 IF H=>20 THEN 480
440 IF H<=3 THEN 480
450 RESET
460 GOTO 590
470
480 IF MOD(N,4)<>0 THEN 520
500 RESET
510 GOTO 590
520 IF MOD(N,2)=0 THEN 560
525 GOSUB 600
530 PRINT TAB(1); D;M1$;H;M;S;"-";X;Y;Z
540 RESET
550 GOTO 590
560 GOSUB 600
565 PRINT TAB(38);D;M1$;H;M;S;"-";X;Y;Z
580 RESET
590 NEXT J
```

EPHEM Page 2.

```
595
600 D4=J*1.00273790852+.186831497
610 G3=D4-INT(D4)
620 X=INT(G3*24)
630 G4=G3*24-X
640 Y=INT(G4*60)
650 G5=G4*60-Y
660 Z=INT(G5*60)
670 RETURN
675
679 PRINT
680 PRINT "END OF MAY"
690 END
Ready
```

AD-A134 182 DETERMINATION OF INDIVIDUAL TEMPERATURES AND LUMINOSITIES IN ECLIPSING BINARY STAR SYSTEMS(U) NAVAL ACADEMY ANNAPOLIS MD R M CAMPBELL 20 JUN 83 USNA-TSPR-122 F/G 3/2 NL

2/2

UNCLASSIFIED

END
DATE FILMED
11 83
DTIC

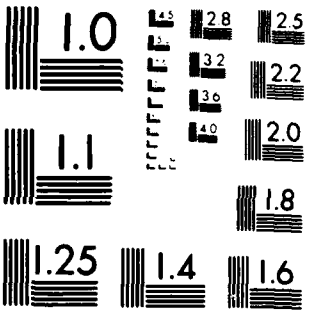

```
YLEYN     27 Apr 83  23:17

! This program, in conjunction with TENSOP, reduces photometric
! data by the multilinear approach of Harris et. al. (PASP, V. 93,
! pp. 297-518) as explained in the text.  This program specifically
! takes photometric data and constructs the Z and S tensors for
! manipulation by TENSOP in double-precision BASIC6.  This program
! utilises BASIC7 so that it may handle third rank tensors.

! Variable assignment is as follows:
! Z and S are reduction co-efficient tensors.
! Y is a dummy composite co-efficient tensor, expressed as a scalar
!    during each loop for storage conservation.
! X is the air mass tensor.
! W is the weighting factor, W=X^-2.5, never explicitly expressed.
! CIP is the published colour index tensor.
! CIO is the observed colour index tensor.
! K is the night index, from 1 to M.
! J is the star index, from 1 to N.
! I and P are indices of Z and S tensors.
! P replaces both I and P in the subprogram TERRI.
! Files STARBV and STARUB store (B-V) and (U-B) data, respectively.

OPEN #BV: "STARBV"
OPEN #UB: "STARUB"
OPEN #TI: "TENSDAT"
DIM Z(83,83), S(83), X(25,40),CIP(25),CIO(25,40)

PRINT "INPUT # OF NIGHTS, # OF STARS";
INPUT M,N
LET L=2*M+3
REDIM Z(L,L),S(L),X(N,M),CIP(N),CIO(N,M)

PRINT "INPUT 1 FOR (B-V), 2 FOR (U-B)";
INPUT R
SELECT
CASE R=1
     RESET #BV
     DO UNTIL END #BV
        INPUT #BV: J$,K$,J,K,X(J,K),CIP(J),CIO(J,K)
     LOOP
CASE R=2
     RESET #UB
     DO UNTIL END #UB
        INPUT #UB: J$,K$,J,K,X(J,K),CIP(J),CIO(J,K)
     LOOP
SELECTEND
```

YLEYN Page 2.

```
! All data tensors are now complete.  Proceed in calculation
! of Z and S tensors.

FOR I=1 TO L
    FOR P=1 TO L
        LET Z(I,P)=0
        LET S(P)=0
        FOR J=1 TO N
            FOR K=1 TO M
                CALL TERRI (I,M,J,K,X(,),CIP(),Yi)
                CALL TERRI (P,M,J,K,X(,),CIP(),Yp)
                SELECT
                CASE X(J,K)<>0
                     LET Z(I,P)=Z(I,P)+Yi*Yp/(X(J,K)^2.5)
                     IF I=L THEN LET S(P)=S(P)+CID(J,K)*Yp/(X(J,K)^2.5)
                CASE X(J,K)=0
                SELECTEND
            NEXT K
        NEXT J
    NEXT P
NEXT I

! Z and S tensors are now complete.  Proceed in transfering
! these to file TENSDAT.

SCRATCH #TI
FOR I=1 TO L
    FOR P=1 TO L
        PRINT#TI: Z(I,P)
    NEXT P
NEXT I
FOR P=1 TO L
    PRINT#TI: S(P)
NEXT P
CLOSE #TI
```

YLEYN Page 3.

```
! Subprogram TERRI calculates reduction co-efficient tensors Y.

SUB TERRI (H,M,J,K,X(,),CIP(),Y)
    SELECT
    CASE H=L
         LET Y=CIP(J)^2
    CASE H=L-1
         LET Y=X(J,K)*CIP(J)
    CASE H=L-2
         LET Y=CIP(J)
    CASE H>M
         IF H=M+K THEN LET Y=X(J,K) ELSE LET Y=0
    DEFAULT
         IF H=K THEN LET Y=1 ELSE LET Y=0
    SELECTEND
SUBEND

END
Ready
```

```
TENSOR    27 Apr 83  23:19

10 ' This program takes the Z and S tensors created in YLEYN,
20 ' and calculates the co-efficient tensor G=Z(-1)*S, which
30 ' is used directly to reduce observations of unknown stars.
40 ' The inversion and accuracy checking subprograms were written
50 ' by Prof. H. Kaplan of the Naval Academy mathematics department
60 ' in 1976.
80
90 ' Variable assignment is as follows:
100 ' Z and S are the reduction co-efficient tensors found in YLEYN.
110 ' V is the inverse of Z
120 ' T is a dummy workspace in subprogram MATINV, and later Z*V.
130 ' G is the co-efficient tensor V*S.
140 ' M is the number of nights observed.
150 ' E is the absolute deviation of T from the identity tensor.
160
170 LIBRARY "BASICLIB***: MATINV"
180 FILE #1: "TENSDAT"
190 DIM Z(83,83),T(83,83),V(83,83),S(83),G(83)
200 PRINT "INPUT # OF NIGHTS";
210 INPUT M
220 L=2*M+3
230
239 RESET #1
240 FOR I=1 TO L
250 FOR P=1 TO L
260 INPUT #1: Z(I,P)
270 NEXT P
280 NEXT I
290 FOR P=1 TO L
300 INPUT #1: S(P)
310 NEXT P
320
330 PRINT "DOEST THOU WISH TO SEE Z AND S";
340 INPUT G$
350 IF G$<>"VERILY" THEN 410
360 CALL "TENSPRI": Z(,),L
370 FOR P=1 TO L
380 PRINT S(P);
390 NEXT P
400 PRINT
410
420 CALL "MATINV": Z(,),T(,),V(,),L
425 PRINT
430 PRINT "DOEST THOU WISH TO SEE Z(-1)";
440 INPUT G$
450 IF G$<>"VERILY" THEN 470
460 CALL "TENSPRI": V(,),L
```

TENSOP Page 2.

```
470
475 PRINT
480 PRINT "DOEST THOU WISH THE ACCURACY OF Z(-1) CONFIRMED";
490 INPUT G$
500 IF G$<>"VERILY" THEN 600
510 CALL "MATGOOD": Z(,),T(,),V(,),L,E
520 PRINT E;"IS THE SUM OF TOTAL ABSOLUTE DEVIATION OF Z*Z(-1)"
530 PRINT "  FROM THE IDENTITY TENSOR."
540 PRINT
550 PRINT "DOEST THOU WISH TO SEE Z*Z(-1)";
560 INPUT G$
570 IF G$<>"VERILY" THEN 600
580 MAT T=Z*V
590 CALL "TENSPRI": T(,),L
595
600 PRINT
605 FOR I=1 TO L
610 G(I)=0
620 FOR P=1 TO L
630 G(I)=G(I)+V(I,P)*S(P)
640 NEXT P
645 NEXT I
650 PRINT "*** FIAT G ***"
655 PRINT
660 FOR I=1 TO L
670 PRINT G(I)
680 NEXT I
690 END
695
700 SUB "TENSPRI": V(,),L
710 PRINT
720 FOR I=1 TO L
730 FOR P=1 TO L
740 PRINT V(I,P);
750 NEXT P
760 PRINT
770 NEXT I
780 PRINT
790 SUBEND
Ready
```

# APPENDIX III

## LIST OF PROGRAM BINARIES

| SYSTEM | α | δ | PER | $h_{max}$ | m | $m_{tot}$ | #TOTALITIES |
|---|---|---|---|---|---|---|---|
| RT And | 23-10-25 | 52-56-02 | 0.629 | 4-39 | 9.5 | 9.7 | 0 |
| TW And | 00-02-25 | 32-45-02 | 4.12 | 4-01 | 9.0 | 11.0 | 0 |
| AA And | 23-04-37 | 47-35-40 | 0.935 | 4-30 | 10.2 | 10.5 | 0 |
| V346 Aqu | 20-09-11 | 10-17-55 | 1.11 | 2-55 | 9.0 | 9.5 | 1 |
| TZ Boo | 15-07-32 | 40-02-01 | 0.297 | 4-16 | 10.5 | 11.0 | 40 |
| AC Boo | 14-55-53 | 46-25-49 | 0.352 | 4-28 | 10.5 | 10.9 | 41 |
| SS Cam | 07-14-21 | 73-21-51 | 4.82 | 4-56 | 10.0 | 10.6 | 4 |
| SV Cam | 06-37-40 | 82-17-14 | 0.593 | 4-28 | 9.0 | 9.1 | 21 |
| SZ Cam | 04-06-19 | 62-17-17 | 2.69 | 4-51 | 7.5 | 7.7 | 2 |
| TU Cam | 05-53-26 | 59-53-09 | 2.93 | 4-48 | 5.5 | 5.6 | 6 |
| S Cnc | 08-42-58 | 19-05-43 | 9.48 | 3-25 | 8.0 | 10.1 | 0 |
| RS CVn | 13-09-50 | 36-01-29 | 4.80 | 4-08 | 8.0 | 9.2 | 3 |
| TW Cas | 02-44-29 | 65-39-21 | 1.43 | 4-54 | 8.5 | 8.6 | 1 |
| TX Cas | 02-50-54 | 62-42-50 | 2.93 | 4-51 | 9.0 | 9.3 | 1 |
| YZ Cas | 00-44-30 | 74-53-46 | 4.47 | 4-55 | 5.5 | 5.6 | 0 |
| AR Cas | 23-29-15 | 58-27-21 | 6.07 | 4-46 | 5.0 | 5.1 | 0 |
| DO Cas | 02-40-05 | 60-28-53 | 0.685 | 4-49 | 8.5 | 8.6 | 3 |
| U Cep | 01-00-44 | 81-47-04 | 2.49 | 4-32 | 7.0 | 9.8 | 0 |
| ZZ Cep | 22-44-28 | 68-02-35 | 1.72 | 4-45 | 9.5 | 10.0 | 0 |
| α CrB | 15-33-58 | 26-46-20 | 17.36 | 3-46 | 2.2 | 2.3 | 1 |
| BR Cyg | 19-40-24 | 46-44-38 | 1.33 | 4-29 | 9.5 | 10.5 | 0 |
| DK Cyg | 21-34-20 | 34-31-11 | 0.471 | 4-05 | 10.5 | 11.1 | 0 |
| KR Cyg | 20-08-25 | 30-30-04 | 0.845 | 3-56 | 9.0 | 9.1 | 2 |
| MR Cyg | 21-58-18 | 45-54-07 | 1.68 | 4-31 | 8.5 | 8.7 | 0 |
| V380 Cyg | 19-50-02 | 40-33-21 | 12.43 | 4-17 | 5.5 | 5.6 | 0 |
| V382 Cyg | 20-18-09 | 36-17-16 | 1.89 | 4-08 | 9.0 | 9.8 | 0 |
| W Del | 20-36-54 | 18-13-27 | 4.81 | 3.22 | 9.5 | 12.5 | 1 |
| DM Del | 20-38-48 | 14-22-02 | 0.845 | 3-10 | 8.5 | 8.7 | 1 |
| SX Dra | 18-04-19 | 58-23-45 | 5-17 | 4-46 | 10.0 | 11.8 | 1 |
| TW Dra | 15-33-36 | 63-57-49 | 2.81 | 4-52 | 7.5 | 9.8 | 5 |
| RW Gem | 06-00-26 | 23-08-27 | 2.87 | 3-37 | 10.0 | 11.8 | 2 |
| RY Gem | 07-26-26 | 15-41-45 | 9.30 | 3-14 | 8.5 | 10.5 | 1 |
| TT Her | 16-53-57 | 16-51-52 | 0.912 | 3-18 | 9.5 | 9.8 | 6 |
| AK Her | 17-13-12 | 16-22-15 | 0.422 | 3-17 | 8.5 | 8.9 | 15 |
| VZ Hya | 08-30-52 | -06-15-40 | 2.90 | 1-08 | 9.0 | 9.5 | 1 |
| AM Leo | 11-01-18 | 09-59-21 | 0.366 | 2-54 | 8.5 | 9.1 | 32 |
| SW Lyn | 08-06-53 | 41-51-03 | 0.644 | 4-20 | 9.5 | 9.8 | 14 |
| TU Mon | 07-52-29 | -02-59-51 | 5.05 | 1.44 | 8.5 | 10.9 | 2 |
| UX Mon | 07-58-27 | -07-27-29 | 5.90 | 0-58 | 8.0 | 8.9 | 0 |
| RV Oph | 17-33-46 | 07-15-30 | 3.69 | 2-42 | 9.5 | 11.5 | 1 |
| V566 Oph | 17-56-02 | 04-59-16 | 0.409 | 2-32 | 7.5 | 7.9 | 8 |
| VV Ori | 05-32-40 | -01-10-09 | 1.49 | 1-57 | 5.0 | 5.2 | 1 |
| EE Peg | 21-39-12 | 09-06-25 | 2.63 | 2-50 | 7.0 | 7.1 | 0 |
| RY Per | 02-44-33 | 48-04-24 | 6.86 | 4-32 | 8.5 | 10.3 | 1 |
| ST Per | 02-59-00 | 39-07-25 | 2.65 | 4-14 | 9.5 | 12.0 | 0 |

| SYSTEM | α | δ | PER | $h_{max}$ | m | $m_{tot}$ | # TOTALITIES |
|---|---|---|---|---|---|---|---|
| U Sge | 19-18-04 | 19-34-45 | 3.38 | 3-27 | 6.5 | 10.1 | 1 |
| RW Tau | 04-02-51 | 28-04-50 | 2.77 | 3-50 | 8.0 | 12.5 | 2 |
| RZ Tau | 04-35-39 | 18-43-15 | 0.416 | 3-24 | 10.5 | 11.1 | 2 |
| X Tri | 01-59-35 | 27-48-23 | 0.972 | 3-49 | 9.0 | 11.4 | 0 |
| W UMa | 09-42-34 | 56-01-49 | 0.334 | 4-43 | 8.5 | 9.2 | 36 |
| AG Vir | 12-00-11 | 13-06-10 | 0.643 | 3-05 | 9.0 | 9.4 | 20 |

## LIST OF STANDARD STARS

| SYSTEM | α | δ | m | (B-V) | (U-B) | SPECTRAL CLASS |
|---|---|---|---|---|---|---|
| θ And | 00-16.3 | 58-35 | 4.60 | +.06 | +.02 | A2V |
| μ Cas | 01-06.6 | 54-53 | 5.12 | .69 | +.09 | G5V |
| β Tri | 02-08.5 | 34-55 | 3.00 | .13 | +.08 | A5III |
| μ Cet | 02-44.0 | 10-03 | 4.25 | .31 | +.05 | F0IV |
| δ Per | 03-41.7 | 47-44 | 3.03 | -.14 | -.52 | B5III |
| 134 Tau | 05-48.6 | 12-39 | 4.91 | -.07 | -.20 | B9IV |
| β Gem | 07-44.3 | 28-04 | 1.15 | 1.00 | +.84 | K0III |
| η Hya | 08-42.5 | 03-28 | 4.31 | -.196 | -.74 | B3V |
| ι UMa | 08-58.1 | 48-07 | 3.12 | .18 | +.06 | A7V |
| 40 Leo | 10-18.8 | 19-34 | 4.83 | .44 | -.01 | F6V |
| β Vir | 11-49.7 | 01-52 | 3.63 | .54 | +.10 | F8V |
| 78 UMa | 13-00.4 | 56-27 | 4.93 | .57 | 0.00 | F2V |
| β Com | 13-11.1 | 27-57 | 4.30 | .56 | +.05 | G0V |
| η Boo | 13-53.8 | 18-29 | 2.70 | .59 | +.20 | G0IV |
| α Dra | 14-04.0 | 64-27 | 3.64 | -.05 | -.09 | A0III |
| α Boo | 14-15.0 | 19-19 | -0.06 | 1.23 | 1.26 | F2III |
| ε CrB | 15-56.8 | 26-56 | 4.15 | 1.227 | 1.28 | K3III |
| τ Her | 16-19.2 | 46-21 | 3.89 | -.155 | -.56 | B5IV |
| δ Her | 17-14.3 | 24-51 | 3.14 | .08 | +.08 | A3IV |
| 72 Her | 17-20.0 | 32-31 | 5.39 | .62 | +.07 | G0V |
| γ Dra | 17-56.2 | 51-29 | 2.22 | 1.52 | 1.86 | K5III |
| α Del | 20-38.7 | 15-52 | 3.77 | -.06 | -.23 | B9V |
| 1 Peg A | 21-21.3 | 19-44 | 4.09 | 1.10 | 1.05 | K1II |
| 55 Peg | 23-06.2 | 09-19 | 4.50 | 1.56 | 1.81 | M2III |
| γ Cep | 23-38.6 | 77-32 | 3.22 | 1.05 | +.92 | K1IV |

# APPENDIX IV

## STANDARD STAR OBSERVATIONS

All of the observations of standard stars made in the course of the project are given in this appendix. The first page is (b-v) data, and the second is (u-b). The order of data is:

Star, Date, Star Index, Night Index, Air Mass, Published Color Index, Observed Color Index

This data was accessed by YLEYN in order to calculate $Z_{\mu\sigma}$ and $S_{\sigma}$.

```
STARBV    27 Apr 83  23:21

bGEM, 31JAN, 1,1, 1.017, 1.0, .81
nHYA, 31JAN, 2,1, 1.246, -.196, .11
bGEM, 8FEB, 1,2, 1.029, 1.0, .82
dPER, 8FEB, 3,2, 1.183, -.14, .06
bGEM, 17FEB, 1,3, 1.041, 1.0, .83
dPER, 17FEB, 3,3, 1.097, -.14, .08
78UMa, 19FEB, 4,4, 1.048, .57, .32
bGEM, 21FEB, 1,5, 1.019, 1.0, .85
iUMa, 21FEB, 5,5, 1.02, .18, .33
134TAU, 2MAR, 6,6 1.164, -.07, .12
bGEM, 2MAR, 1,6, 1.021, 1.0, .81
iUMA, 2MAR, 5,6, 1.013, .18, .20
bVIR, 2MAR, 7,6, 1.289, .54, .52
bGEM, 15MAR, 1,7, 1.080, 1.0, .76
iUMa, 15MAR, 5,7, 1.025, .18, .16
78UMa, 15MAR, 4,7, 1.063, .57, .36
40LEO, 15MAR, 8,7, 1.061, .44, .41
bCOM, 15MAR, 9,7, 1.019, .56, .51
iUMa, 23MAR, 5,8, 1.019, .18, .21
nBOO, 23MAR, 10,8, 1.075, .59, .54
aDRA, 23MAR, 11,8, 1.109, -.05, .02
eCrB, 23MAR, 12,8, 1.024, 1.227, 1.05
bGEM, 4APR, 1,9, 1.087, 1.0, .80
40LEO, 4APR, 8,9, 1.072, .44, .42
bVIR, 12APR, 7,10, 1.253, .54, .836
bCOM, 12APR, 9,10, 1.019, .56, .555
nBOO, 12APR, 10,10, 1.068, .59, .543
eCrB, 12APR, 12,10, 1.023, 1.227, 1.084
aDRA, 16APR, 11,11, 1.141, -.05, .062
bCOM, 16APR, 9,11, 1.019, .56, .524
tHER, 16APR, 13,11, 1.16, -.155, -.018
dHER, 16APR, 14,11, 1.261, .08, .127
aDRRA, 16APR, 15,11, 1.072, 1.52, 1.228
72HER, 16APR, 16,11, 1.009, .62, .557
eCrB, 20APR, 12,12, 1.093, 1.227, 1.106
dHER, 20APR, 14,12, 1.031, .08, .11
aDRA, 20APR, 15,12, 1.029, 1.52, 1.23
dHER, 21APR, 14,13, 1.041, .08, .136
aDRA, 21APR, 15,13, 1.036, 1.52, 1.282
72HER, 21APR, 16,13, 1.007, .62, .642
Ready
```

```
STARUB    27 Apr 83  23:22

bGEM 31JAN, 1,1, 1.017, .84, 2.51
nHYA, 31JAN, 2,1, 1.246, -.74, 1.03
bGEM, 8FEB, 1,2, 1.029, .84, 2.56
dPER, 8FEB, 3,2, 1.183, -.52, 1.38
bGEM, 17FEB, 1,3, 1.041, .84, 2.62
dPER, 17FEB, 3,3, 1.097, -.52, 1.25
78UMa, 19FEB, 4,4, 1.048, 0.0, 1.76
bGEM, 21FEB, 1,5, 1.019, .84, 2.63
iUMa, 21FEB, 5,5, 1.02, .08, 1.79
134TAU, 2MAR, 6,6, 1.164, -.20, 1.58
bGEM, 2MAR, 1,6, 1.021, .84, 2.53
iUMA, 2MAR, 5,6, 1.013, .08, 1.77
bVIR, 2MAR, 7,6, 1.289, .10, 1.82
bGEM, 15MAR, 1,7, 1.08, .84, 2.55
iUMa, 15MAR, 5,7, 1.025, .08, 1.76
78UMa, 15MAR, 4,7, 1.063, 0.0, 1.7
40LEO, 15MAR, 8,7, 1.061, -.01, 1.74
bCOM, 15MAR, 9,7, 1.019, .05, 1.98
iUMa, 23MAR, 5,8, 1.019, .08, 1.73
nBOO, 23MAR, 10,8, 1.075, .20, 1.88
aDRA, 23MAR, 11,8, 1.109, -.09, 1.58
eCrB, 23MAR, 12,8, 1.024, 1.28, 2.95
bGEM, 4APR, 1,9, 1.087, .84, 2.56
40LEO, 4APR, 8,9, 1.072, -.01, 1.75
bVIR, 12APR, 7,10, 1.253, .10, 1.96
bCOM, 12APR, 9,10, 1.019, .05, 1.83
nBOO, 12APR, 10,10, 1.068, .20, 1.98
eCrB, 12APR, 12,10, 1.023, 1.28, 2.98
aDRA, 16APR, 11,11, 1.141, -.09, 1.611
bCOM, 16APR, 9,11, 1.019, .05, 1.741
tHER, 16APR, 13,11, 1.16, -.56, 1.22
dHER, 16APR, 14,11, 1.261, .08, 1.782
aDRA, 16APR, 15,11, 1.072, 1.86, 3.533
72HER, 16APR, 16,11, 1.009, .07, 1.795
eCrB, 20APR, 12,12, 1.093, 1.28, 2.975
dHER, 20APR, 14,12, 1.031, .08, 1.732
aDRA, 20APR, 15,12, 1.029, 1.86, 3.563
dHER, 21APR, 14,13, 1.041, .08, 1.749
aDRA, 21APR, 15,13, 1.036, 1.86, 3.62
72HER, 21APR, 16,13, 1.007, .07, 1.817
Ready
```

UNCLASSIFIED

SECURITY CLASSIFICATION OF THIS PAGE (When Data Entered)

| REPORT DOCUMENTATION PAGE | READ INSTRUCTIONS BEFORE COMPLETING FORM |
|---|---|
| 1. REPORT NUMBER: U.S.N.A. - TSPR; no. 122 (1983) | 2. GOVT ACCESSION NO.: A134 182 — 3. RECIPIENT'S CATALOG NUMBER: |
| 4. TITLE (and Subtitle): DETERMINATION OF INDIVIDUAL TEMPERATURES AND LUMINOSITIES IN ECLIPSING BINARY STAR SYSTEMS. | 5. TYPE OF REPORT & PERIOD COVERED: Final: 1982/1983 |
| | 6. PERFORMING ORG. REPORT NUMBER: |
| 7. AUTHOR(s): Campbell, Robert M. | 8. CONTRACT OR GRANT NUMBER(s): |
| 9. PERFORMING ORGANIZATION NAME AND ADDRESS: United States Naval Academy, Annapolis. | 10. PROGRAM ELEMENT, PROJECT, TASK AREA & WORK UNIT NUMBERS: |
| 11. CONTROLLING OFFICE NAME AND ADDRESS: United States Naval Academy, Annapolis. | 12. REPORT DATE: 20 June 1983 — 13. NUMBER OF PAGES: 103 |
| 14. MONITORING AGENCY NAME & ADDRESS(if different from Controlling Office): | 15. SECURITY CLASS. (of this report): UNCLASSIFIED — 15a. DECLASSIFICATION/DOWNGRADING SCHEDULE: |

16. DISTRIBUTION STATEMENT (of this Report)

This document has been approved for public release; its distribution is UNLIMITED.

17. DISTRIBUTION STATEMENT (of the abstract entered in Block 20, if different from Report)

This document has been approved for public release; its distribution is UNLIMITED.

18. SUPPLEMENTARY NOTES

Accepted by the U. S. Trident Scholar Committee.

19. KEY WORDS (Continue on reverse side if necessary and identify by block number)

Photometry, Astronomical
Stars, Double
Eclipsing binaries

20. ABSTRACT (Continue on reverse side if necessary and identify by block number)

The purpose of this project was to determine the temperatures and luminosities of the individual components of eclipsing binary star systems. Dr. Richard L. Walker of the U. S. Naval Observatory provided a list of such systems which were as yet undetermined. The information sought was gained by UBV photometry of a system at total eclipse and at a time outside eclipse. The light at totality is due entirely to the occulting star, and outside eclipse, both stars contribute fully.

(OVER)

DD FORM 1 JAN 73 1473 EDITION OF 1 NOV 65 IS OBSOLETE
S/N 0102-LF-014-6601

UNCLASSIFIED

SECURITY CLASSIFICATION OF THIS PAGE (When Data Entered)

A method is derived for subtracting out the light of the occulting star to obtain measurements of the occulted.

A recently published technique by William E. Harris was used to reduce raw observational data. Essentially a simultaneous, multi-linear solution for both atmospheric extinction and instrumental transformation, this method was programmed onto the Naval Academy's extensive computing facilities. It was found that this method, as claimed, gives accurate results with a minimum of time and effort, upon completion of the initial phase of programming.

Systems for which a complete solution (temperature and luminosity of both components) was reached include: TUC Camelopardi, TW Draconis, AK Herculis, V566 Ophiuchi, W Ursae Majoris, and AG Virginis. Sustems observed only during totality, thus solving only the occulting star, include a Corona Borealis and AM Leonis. RS Canes Venactici and TZ Bootes were observed only out of eclipse, and must await further study. Once a solution for a system was obtained, it was presented graphically on a Hertzsprung-Russell diagram, and was examined from the viewpoint of binary evolution.

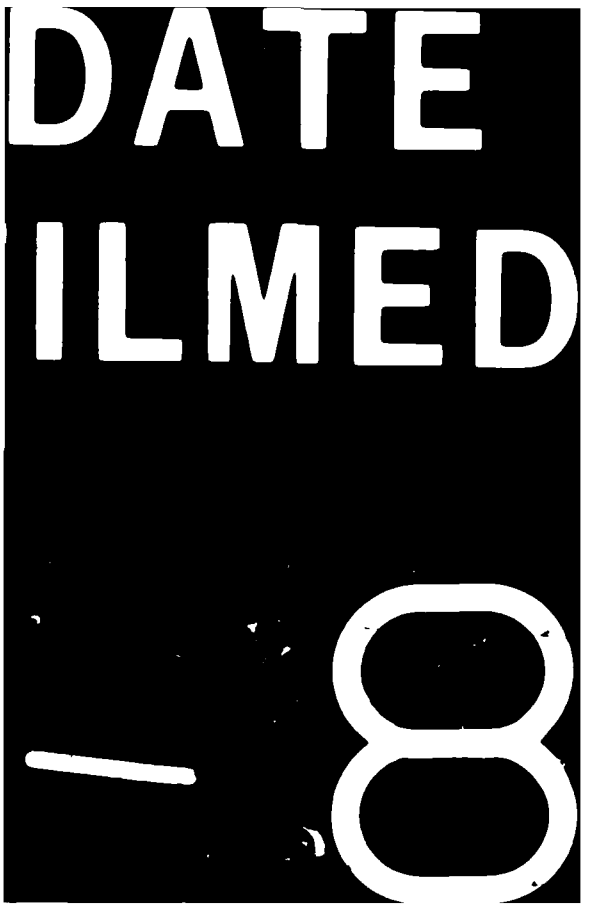
DATE
ILMED
8